Synthesis, crystal structure, Deoxyribose Nucleic Acid interaction and antitumor activity of some thiosemicarbazonatomolybdenum(VI)

Mouayed A. Hussein, Teoh S. Guan, Rosenani A. Haque, Mohamed B. Khadeer Ahamed, Amin M.S. Abdul Majid

PII: S0020-1693(14)00209-6
DOI: http://dx.doi.org/10.1016/j.ica.2014.04.005
Reference: ICA 15944

To appear in: *Inorganica Chimica Acta*

Received Date: 16 October 2013
Revised Date: 13 March 2014
Accepted Date: 14 April 2014

Please cite this article as: M.A. Hussein, T.S. Guan, R.A. Haque, M.B. Khadeer Ahamed, A.M.S. Abdul Majid, Synthesis, crystal structure, Deoxyribose Nucleic Acid interaction and antitumor activity of some thiosemicarbazonatomolybdenum(VI), *Inorganica Chimica Acta* (2014), doi: http://dx.doi.org/10.1016/j.ica.2014.04.005

Synthesis, crystal structure, Deoxyribose Nucleic Acid interaction and antitumor activity of some thiosemicarbazonatomolybdenum(VI)

Mouayed A. Hussein [a], Teoh S. Guan [a *], Rosenani A. Haque [a], Mohamed B. Khadeer Ahamed[b], Amin M.S. Abdul Majid[b]

[a] School of Chemical Science, Universiti Sains Malaysia, 11800 – Mindern, Pulau Pinang, Malaysia

[b] EMAN Research and Testing Laboratory, School of Pharmaceutical Sciences, Universiti Sains Malaysia, 11800 – Mindern, Pulau Pinang, Malaysia

*Corresponding author: Dr. Teoh Siang Guan, PhD,
Professor
School of Chemical Sciences
Universiti Sains Malaysia
Penang-11800, Malaysia
E-mail: sgteoh@usm.my
H/P : (604) – 6577888
Fax : (604) - 6574854

Abstract

Four dioxomolybdenum(VI) complexes were synthesized by reacting $[MoO_2(acac)_2]$ with thiosemicarbazone ligands derived from 5-chloro-2-hydroxybenzaldehyde (**H_2L_1**),

2-hydroxy-5-methylbenzaldehyde (**H_2L_2**), 3-tert-butyl-2-hydroxybenzaldehyde (**H_2L_3**), or 2,3-dihydroxybenzaldehyde (**H_2L_4**). In all the complexes, the ligands were coordinated to molybdenum as tridentate ONS donors. X-ray crystallography showed that the distorted octahedral coordination of molybdenum atom is completed by methanol molecule (D) as in **[$MoO_2(L_1D)$]**, **[$MoO_2(L_2D)$]**, and **[$MoO_2(L_3D)$],** or by an ethanol molecule as in **[$MoO_2(L_4D)$]**. The molecular structures of **H_2L_2**, **H_2L_3**, and all synthesized complexes were determined via single crystal X-ray crystallography. The binding properties of the ligand and the complexes with calf thymus DNA were analyzed by UV, fluorescence titration, and viscosity measurements. Gel electrophoresis shows that all complexes can cleave the pBR322 plasmid DNA. The cytotoxic properties of the complexes were studied against human colorectal cell lines. All complexes showed strong antiproliferative activities in the relative order **[$MoO_2(L_3D)$] > [$MoO_2(L_1D)$] ~ [$MoO_2(L_2D)$] > [$MoO_2(L_4D)$]** with IC_{50} values of 3.2, 4.5, 4.6, and 6.4 μM, respectively. The complexes exhibited greater pronounced activity than the standard reference drug, 5-fluorouracil, did (IC_{50} = 7.3 μM). These studies demonstrate the potential application of dioxomolybdenum (VI) complexes in chemotherapy.

Key words: Thiosemicarbazone, Molybdenum(VI) complexes, X-ray crystal structure, DNA binding, DNA cleavage, Antiproliferative activity

1. Introduction

Thiosemicarbazones, which are important groups of compounds, have attracted much research interest because of their substantial biological and pharmacological properties such as antiviral, antibacterial, and antifungal activities [1,2]. The actions of thiosemicarbazones display remarkable activities when coordinated with metal ions [3–5].

Molybdenum has been broadly investigated recently because of its essential role in almost all biological systems. Molybdenum participates in a wide range of metalloenzymes called molybdoenzymes, in which molybdenum forms a part of the active sites of these enzymes [6,7]. These enzymes utilize molybdenum as a cofactor that catalyzes the transformation processes such as in sulfite oxidase [8], xanthine oxidase [9], and aldehyde oxidase [10]. Molybdenum(VI) complexes with thiosemicarbazones serving as ONS donor ligands have been regarded as excellent models for the molybdenum binding site of these enzymes [11–15].

In this study, a series of *cis*-dioxomolybdenum(VI) complexes with thiosemicarbazone ligands were synthesized and characterized (Scheme 1). The complexes and their respective ligands were tested for DNA cleaving/binding by spectral and physical methods. Moreover, the complexes were tested against human colorectal (HCT 116) cell lines. The structures of all complexes were described in detail by X-ray crystallography.

2. Experimental

2.1. Materials and methods

Melting point was measured by the Stuart Scientific SMP1 melting point apparatus. Infrared (IR) spectra were recorded by the Perkin Elmer System 2000 spectrophotometer by using the KBr disc method. The nuclear magnetic resonance (NMR) spectra of ^{1}H and ^{13}C were recorded by a Bruker 500 MHz and 400 MHz, respectively, with tetramethylsilane serving as an internal standard and DMSO-d_6 serving as the solvent. Elemental analysis was conducted by the Perkin Elmer 2400 Series-11 CHN analyzer. Electronic and fluorescent spectra were recorded by Perkin Elmer Lambda-35 and Jasco FP-750 spectrophotometers, respectively. X-ray crystallographic data were recorded on a Bruker SMART APEXII CCD area-detector diffractometer using graphite monochromated Mo Kα radiation (λ = 0.71073 A^0) at 100 K.

The data were collected and reduced using APEX2 and SAINT programs. The structure of all compounds was solved using the SHELXS-97 program package, and refined using the SHELXL-97 program package [16]. All non-hydrogen atoms were anisotropically refined. The molecular graphics were created using SHELXTL-97. All chemicals, including thiosemicarbazide, aldehydes, and the solvents, were purchased from Sigma-Aldrich.

2.2. Synthesis of ligands

2.2.1. Synthesis of *N*-methyl-2-(5-chloro-2-hydroxybenzylidene) hydrazinecarbothioamide (**H_2L_1**)

A solution of 5-chloro-2-hydroxybenzaldehyde (0.74 g, 4.75 mmol) in ethanol (20 ml) was added to a solution of 4-methyl-3-thiosemicarbazide (0.5 g, 4.75 mmol) in ethanol (20 ml). The resulting yellow solution was refluxed with stirring. After 1 h, a pale yellow solid was formed, which was then filtered, washed with ethanol, and air-dried. Mp: 234 °C to 236 °C, (0.80 g, 70%). Anal. Calcd for $C_9H_{10}ClN_3OS$: C, 44.41; H, 4.11; N, 17.27. Found: C, 44.21; H, 4.13; N, 17.09 (%); IR(KBr) (ν_{max}/cm^{-1}): 3398 (s, NH), 3125 (m, OH), 1600–1615 (m, C=N–N–C), 1553 (m, $C_{aro}O$), 1271 (m, C=S); ^{1}H NMR (DMSO-d_6, ppm): 3.01 (s, CH_3), 6.87, 7.25, 8.06 (d, d, s, H-aromatic), 8.30 (s, CS–NH), 8.58 (s, CH=N), 10.25 (OH), 11.47 (s, N–NH). ^{13}C NMR (DMSO–d_6, ppm): 30.80 (CH_3), 117.71–136.96 (C-aromatic), 155.06 (C=N), 177.66 (C=S).

2.2.2. Synthesis of *N*-ethyl-2-(5-methyl-2- hydroxybenzylidene) hydrazinecarbothioamide (**H_2L_2**)

A solution of 5-methyl-2-hydroxybenzaldehyde (0.57 g, 4.19 mmol) in ethanol (20 ml) was added to a solution of 4-ethyl-3-thiosemicarbazide (0.5 g, 4.19 mmol) in ethanol (20 ml). The resulting colorless solution was refluxed with stirring. After 1 h, a white solid was formed, which was then filtered, washed with ethanol, and air-dried. Colorless needle crystals were

obtained through the slow evaporation of ethanol solution at room temperature. Mp: 164 °C to 166 °C, (0.72 g, 73%). Anal. Calcd for $C_{11}H_{15}N_3OS$: C, 55.61; H, 6.32; N, 17.69. Found: C, 54.16; H, 6.31; N, 17.91 (%); IR(KBr) (ν_{max}/cm^{-1}): 3351–3285 (s, NH), 1601 (m, C=N), 1548 (s, $C_{aro}O$), 1273 (m, C=S); ^1H NMR (DMSO-d_6, ppm): 1.05 (t, CH_3), 2.23 (s, H_3C–Ph), 3.60 (dd, CH_2), 6.76, 7.03, 7.70 (d, d, s, H-aromatic), 8.35 (s, CS–NH), 8.40 (s, CH=N), 9.65(OH), 11.31 (s, N–NH); ^{13}C NMR (DMSO–d_6, ppm): 14.62 (CH_3), 20.07 (CH_3–Ph), 30.62 (CH_2), 115.94–141.53 (C-aromatic), 154.24 (C=N), 176.50 (C=S).

2.2.3. Synthesis of *N*-ethyl-2-(3-ter-butyl-2- hydroxybenzylidene) hydrazinecarbothioamide (**H_2L_3**)

A solution of 3-ter-butyl-2-hydroxybenzaldehyde (0.74 g, 4.19 mmol) in ethanol (20 ml) was added to a solution of 4-ethyl-3-thiosemicarbazide (0.5 g, 4.19 mmol) in ethanol (20 ml). The resulting colorless solution was refluxed with stirring for 2 h and then filtered. The filtrate was left to stand at room temperature for 2 d. Colorless block crystals were obtained. Mp: 171 °C to 173 °C, (0.93 g, 80%). Anal. Calcd for $C_{14}H_{21}N_3OS$: C, 60.12; H, 7.51; N, 15.03. Found: C, 59.72; H, 7.97; N, 15.04 (%); IR(KBr) (ν_{max}/cm^{-1}): 3411 (m, NH), 3176 (m, OH), 1598 (s, C=N), 1544 (s, $C_{aro}O$), 1268 (m, C=S); ^1H NMR (DMSO-d_6, ppm): 1.11 (t, CH_3), 1.40 {s, $(CH_3)_3$}, 3.59 (dd, CH_2), 6.86, 7.28 (t, dd, H-aromatic), 8.29 (s, CS–NH), 8.51 (s, CH=N), 11.28 (s, N–NH); ^{13}C NMR (DMSO-d_6, ppm): 14.44 (CH_3), 29.35 {$(CH_3)_3$}, 30.63 {$\underline{C}(CH_3)_3$}, 34.46 (CH_2), 118.77–146.61 (C-aromatic), 155.19 (C=N), 176.49 (C=S).

2.2.4. Synthesis of *N*-methyl-2-(2,3-dihydroxybenzylidene) hydrazinecarbothioamide (**H_2L_4**)

A solution of 2,3-dihydroxybenzaldehyde (0.65 g, 4.75 mmol) in ethanol (20 ml) was added to a solution of 4-methyl-3-thiosemicarbazide (0.5 g, 4.75 mmol) in ethanol (20 ml). The resulting pink solution was refluxed with stirring for 2 h. A white fluffy product was formed when the solution was cooled down to room temperature. The resulting product was then

filtered, washed with ethanol, and air-dried. Mp: 240 °C to 242 °C, (0.89 g, 84%). Anal. Calcd for $C_9H_{11}N_3O_2S$: C, 47.94; H, 4.88; N, 18.64. Found: C, 48.00; H, 4.68; N, 18.52 (%); IR(KBr) (ν_{max}/cm^{-1}): 3451 (m, NH), 3147 (m, OH), 1610 (m, C=N), 1546–1529 (s, $C_{aro}O$), 1267 (s, C=S). ^1H NMR (DMSO-d_6, ppm): 3.00 (s, CH_3), 6.64, 6.84, 7.37 (t,d,d, H-aromatic), 8.37 (s, CS–NH), 8.90–9.55 (s, s, OH), 11.39 (s, N–NH). ^{13}C NMR (DMSO–d_6, ppm): 30.62 (CH_3), 116.32–145.12 (C-aromatic), 145.54 (C=N), 177.56 (C=S).

2.3. Synthesis of complexes

2.3.1. Synthesis of *N*-methyl-2-(5-chloro-2-hydroxybenzylidene) hydrazinecarbothioamide dioxomolybdenum(VI) **[$MoO_2(L_1D)$]**

A solution of $MoO_2(acac)_2$ (0.134 g, 0.411 mmol) in methanol (25 ml) was added to a solution of *N*-methyl-2-(5-chloro-2-hydroxybenzylidene) hydrazine carbothioamide (0.1 g, 0.411 mmol) in methanol (25 ml). The resulting red solution was refluxed for 2 h and then filtered. The filtrate was left to stand at room temperature for 3 d. Orange block crystals were obtained. Mp: 244°C to 246 °C, (0.12 g, 75%). Anal. Calcd for $C_{10}H_{11}ClMoN_3O_4S$: C, 29.94; H,2.74; N, 10.48 ; Mo, 23.94. Found: C, 29.08; H, 1.99; N, 10.52; Mo, 23.69 (%); IR(KBr) (ν_{max}/cm^{-1}): 3397 (m, NH), 1595 (s, C=N), 1550 (m, $C_{aro}O$), 938,902 (s, Mo=O).

2.3.2. Synthesis of *N*-ethyl-2-(5-methyl-2-hydroxybenzylidene) hydrazinecarbothioamide dioxomolybdenum(VI) **[$MoO_2(L_2D)$]**

A solution of $MoO_2(acac)_2$ (0.137 g, 0.421 mmol) in methanol (25 ml) was added to a solution of *N*-ethyl-2-(5-methyl-2-hydroxybenzylidene) hydrazine carbothioamide (0.1 g, 0.421 mmol) in methanol (25 ml). The resulting red solution was refluxed for 2 h and then filtered. The filtrate was left to stand at room temperature for 5 d. Brown needle crystals were obtained. Mp: 211 °C to 213 °C, (0.13 g, 83%). Anal. Calcd for $C_{12}H_{17}MoN_3O_4S$: C, 36.42;

H, 4.30; N, 10.62; Mo, 24.27. Found: C, 35.93; H, 3.38; N, 10.58; Mo, 23.97 (%); IR(KBr) (ν_{max}/cm^{-1}): 3382 (s, NH), 1590 (m, C=N), 1560 (s, $C_{aro}O$), 934,896 (s, Mo=O).

2.3.3. Synthesis of *N*-ethyl-2-(3-ter-butyl-2- hydroxybenzylidene) hydrazinecarbothioamide dioxomolybdenum(VI) **[$MoO_2(L_3D)$]**

A solution of $MoO_2(acac)_2$ (0.116 g, 0.357 mmol) in methanol (25 ml) was added to a solution of *N*-ethyl-2-(3-ter-butyl-2-hydroxybenzylidene) hydrazine carbothioamide (0.1 g, 0.357 mmol) in methanol (25 ml). The resulting red solution was refluxed for 2 h and then filtered. The filtrate was left to stand at room temperature for 4 d. Orange block crystals were obtained. Mp: 196 °C to 198 °C, (0.14 g, 90%). Anal. Calcd for $C_{15}H_{23}MoN_3O_4S$: C, 41.15; H, 5.25; N, 9.60; Mo, 21.94. Found: C, 41.04; H, 5.06; N, 9.53; Mo, 21.75 (%); IR(KBr) (ν_{max}/cm^{-1}): 3333 (m, NH), 1596 (m, C=N), 1284 (m, C-S), 934,875 (s, Mo=O).

2.3.4. Synthesis of *N*-methyl-2-(2,3-dihydroxybenzylidene) hydrazinecarbothioamide dioxomolybdenum(VI) **[$MoO_2(L_4D)$]**

A solution of $MoO_2(acac)_2$ (0.144 g, 0.443 mmol) in ethanol (25 ml) was added to a solution of *N*-methyl-2-(2,3-dihydroxybenzylidene) hydrazine carbothioamide (0.1 g, 0.443 mmol) in ethanol (25 ml). The resulting red solution was refluxed for 2 h and then filtered. The filtrate was left to stand at room temperature for 5 d. Brown block crystals were obtained. Mp: 244 °C to 246 °C, (0.15 g, 89%). Anal. Calcd for $C_{11}H_{15}MoN_3O_5S$: C, 33.22; H, 3.77; N, 10.57; Mo, 24.15. Found: C, 31.76; H, 3.37; N, 10.44; Mo, 24.02 (%); IR(KBr) (ν_{max}/cm^{-1}): 3386 (s, NH), 1602 (s, C=N), 1572 (s, $C_{aro}O$), 1266 (m, C-S), 932,902 (s, Mo=O).

2.4. DNA binding study

The binding of complexes with calf thymus DNA (CT DNA) were conducted in a 6.3 mM Tris-HCl/50 mM NaCl buffer (pH 7). The DNA stock solution was prepared by dissolving a suitable amount of DNA in 6.3 mM Tris-HCl/50 mM NaCl buffer (pH 7) at room temperature, which was then stored in a refrigerator for 2 d. The CT DNA solution in the buffer presented a ratio of 1.9:1 for UV absorbance at 260 and 280 nm, suggesting that the DNA was sufficiently free of protein. The DNA concentration was estimated by UV absorbance at 260 nm by using the known molar absorption coefficient value of 6600 $M^{-1}cm^{-1}$ [17]. The UV-Vis spectra were scanned in the wavelength range of 230 nm to 600 nm by using the Tris/HCl buffer solution as a reference.

Fluorescence emission assay was carried out by using the above method. Fluorescence spectra were scanned in the wavelength range of 200 nm to 800 nm by using the Tris/HCl buffer solution as a reference.

Viscosity measurements were obtained by the Cannon Manning Semi-Micro viscometer immersed in thermostatic water bath at 37 °C. Flow times were measured manually with a digital stopwatch. Viscosity values were calculated from the observed flow time of DNA-containing solutions (t) corrected by observed flow time of the solvent mixture used (t_0), $\eta = t - t_0$. Viscosity data were presented as $(\eta/\eta_0)^{1/3}$ versus the ratio of the concentration (r) of the ligand or complex-DNA solutions, where η and η_0 represent the viscosity of the complex in the presence of DNA and the viscosity of the DNA alone, respectively [18].

2.5. DNA cleavage study

The activity of the ligands and the complexes to cleave the pBR322 plasmid DNA was studied by agarose gel electrophoresis in a Tris/EDTA buffer solution. The samples were

incubated at 37 °C for 2 h, treated with loading dye, and electrophoresed for 1 h at 50 V on 1% agarose gel. The gel was then stained with ethidium bromide prior to being photographed under UV light.

2.6. Cytotoxicity study

2.6.1. Preparation of cell culture

HCT 116 cancer cells were grown under optimal incubator conditions. The cells that reached a confluency of 70% to 80% were selected for cell plating purposes. The old medium was replaced through aspiration. The cells were then washed with sterile phosphate buffered saline (pH 7.4) for two to three times. The intact layer of the attached cells was then subjected to trypsinization. The cells were incubated at 37 °C in 5% CO_2 for 3 min to 5 min. The flasks containing the cells were gently tapped to aid cell segregation and were observed under an inverted microscope to determine cell segregation completeness. Trypsin activity was inhibited by adding 5 ml of fresh complete media supplied with 10% fetal bovine serum. The cells were counted and diluted to obtain a final concentration of 2.5×10^5 cells/ml, which were then inoculated into wells (100 µl/well). Finally, the plates containing the cells were incubated at 37 °C with an internal atmosphere of 5% CO_2.

2.6.2. 3-[4,5-dimethylthiazol-2-yl]-2,5-diphenyl tetrazolium bromide (MTT) assay

The cytotoxicity against HCT 116 cells was evaluated by 3-[4,5-dimethylthiazol-2-yl]-2,5-diphenyl tetrazolium bromide (MTT) assay [19]. HCT 116 cells (1.5×10^5 cells/ml, 100 µl/well) were seeded in a 96-well microtiter plate. The plate was incubated overnight in a CO_2 incubator to stimulate cell attachment. Approximately 100 µl of test substance was added into each well. The test substance was diluted with media into the desired concentrations from the stock. The plates were incubated at 37 °C with an internal atmosphere of 5% CO_2 for 72 h. After treatment, 20 µl of MTT reagent was added into each well, and the plates were further

incubated for 4 h. Afterward, 50 µL of MTT lysis solution (DMSO) was added into each well, and the plates were further incubated for 5 min in the CO_2 incubator. Finally, the plates were read at 570 and 620 nm wavelengths by a standard enzyme-linked immunosorbent assay microplate reader. The data were recorded and analyzed to assess the effects of the test substance on the cell viability percentage of growth inhibition. Growth inhibition was calculated from the optical density (OD) obtained from the MTT assay, i.e., the hundredth multiple of the subtracted OD value of control and survived cells over the OD of control cells. Statistical differences between the treatments and the control were evaluated using ANOVA, followed by Tukey's multiple comparison tests. The differences were considered significant at $p<0.05$ and $p<0.01$.

3. Results and discussion

3.1. Synthesis of complexes

New dioxomolybdenum(VI) complexes were obtained by reacting $[MoO_2(acac)_2]$ with 4-methyl(ethyl)thiosemicarbazone ligands derived from 5-chloro-2-hydroxybenzaldehyde (**H_2L_1**), 2-hydroxy-5-methylbenzaldehyde (**H_2L_2**), 3-tert-butyl-2-hydroxybenzaldehyde (**H_2L_3**), or 2,3-hydroxybenzaldehyde (**H_2L_4**). In all complexes, molybdenum coordinated to the ligands as tridentate ONS donors through phenolic-oxygen, imine-nitrogen, and thiol-sulphur. The sixth coordination site (**D**) required to complete the octahedral coordination of molybdenum was occupied by the solvent molecule. X-ray crystallography demonstrated that the **D** site of the distorted octahedral complexes of *cis*-dioxomolybdenum(VI) was occupied by CH_3OH when methanol was used as solvent, such as in **[$MoO_2(L_1D)$]**, **[$MoO_2(L_2D)$]**, and **[$MoO_2(L_3D)$]**, and by CH_3CH_2OH when ethanol (97%) was used as solvent, such as in **[$MoO_2(L_4D)$]**. All ligands and their respective complexes are air-stable and are highly soluble in DMSO and DMF.

The Fourier transform infrared spectroscopy (FTIR), ^{1}H NMR, and ^{13}C NMR spectra, as well as the elemental analysis, exhibited by the ligands (**H_2L_1–H_2L_4**) were all consistent with the assigned structures. In FTIR, the bands in the 1598 cm^{-1} to 1610 cm^{-1} range can be attributed to the (C=N) group, the bands in the 1544 cm^{-1} to 1553 cm^{-1} range can be attributed to the (C_{aro}–O) group, and the bands in the 1267 cm^{-1} to 1273 cm^{-1} range can be attributed to the (C=S) group. In the ^{1}H NMR, the signal caused by the (–CH_3) group of **H_2L_1** and **H_2L_4** emerged at 3.00 ppm, whereas that of **H_2L_2** and **H_2L_3** emerged in the 1.05 ppm to 1.11 ppm range. The signal caused by the (CS–NH) group emerged in the 8.29 ppm to 8.37 ppm range. The signals that emerged in the 6.64 ppm to 8.06 ppm range can be attributed to the aromatic protons, whereas the signals in the 11.28 ppm to 11.47 ppm range can be attributed to the (N–NH) group. In the ^{13}CNMR, the signal caused by the (C=S) group appeared in the 176.49 ppm to 177.66 ppm range. The signal caused by the (C=N) group appeared in the 145.45 ppm to 155.54 ppm range. The signals caused by the aromatic carbons appeared in the 115.94 ppm to 146.61 ppm range.

All complexes (**[$MoO_2(L_1D)$]–[$MoO_2(L_4D)$]**) presented single crystals. The FTIR spectra and elemental analysis were consistent with the assigned structures. In FTIR, a very sharp two bands attributed to the (Mo=O) groups appeared in the 875 cm^{-1} to 938 cm^{-1} range. The data for all compounds are given in the experimental section.

3.2. Crystallographic studies

The crystal and molecular structure of two ligands (**H_2L_2** and **H_2L_3**) and all complexes (**[$MoO_2(L_1D)$]–[$MoO_2(L_4D)$]**) were obtained by using the single crystal X-ray diffraction method. The general crystal data for ligands and complexes are listed in Tables 1 and 2, the relevant bond distances and angles are presented in Tables 3 and 4, respectively, and the molecular structures are presented in Figs. 1–6.

The molecular structures of **H_2L_2** and **H_2L_3** (Figs. 1 and 2) show the *trans* configuration of the S1 atom relating to N1, which is in the *cis* configuration relating to N3. In the free ligand, the S1–C8 bond lengths of 1.702 (7) A^0 (**H_2L_2**) and 1.6840 (18) A^0 (**H_2L_3**) and the N2–C8 bond lengths of 1.337 (8) A^0 (**H_2L_2**) and 1.358 (3) A^0 (**H_2L_3**) were observed, indicating that the ligands were in the tautomeric thione form –NH–C=S. By contrast, the relative molybdenum complexes **[$MoO_2(L_2D)$]** (Fig. 4) and **[$MoO_2(L_3D)$]** (Fig. 5) demonstrate that the meridional coordination plane alters the S1–C8 bond lengths, which become 1.7545 (15) A^0 and 1.7528 (14) A^0, and the N2–C8 bond lengths, which become 1.3156 (19) A^0 and 1.3192 (18) A^0, with respect to the tautomeric thione form –N=C–S. Molybdenum has a distorted octahedral coordination in all complexes (Figs. 3–6). The schiff base ligand bonded to the *cis*-MoO_2^{+2} ion through the phenolate oxygen O1 {O4 in **[$MoO_2(L_3D)$]**}, the imine nitrogen N1, and the thiolate sulfur S1. An oxo group O3 lay *trans* to N1, whereas the other oxo group O2 {O4 in **[$MoO_2(L_1D)$]** and **[$MoO_2(L_4D)$]**} lay *trans* to the **D** group occupied by CH_3OH or CH_3CH_2OH in **[$MoO_2(L_4D)$]**. The bond lengths of the doubly bonded terminal oxo ligands were in the range of 1.6975 (13) A^0 to 1.7157(8) A^0. These ligands had a high O_{oxo}–Mo–O_{oxo} angle of 105.58(6)° because of the repulsion force between them, which is responsible for the elongation of the Mo–D bond from 2.3207 (9) A^0 to 2.3364 (11) A^0 and for the rather weak coordination to the MoO_2^{+2} unit [17].

3.3. Interaction with DNA

3.3.1. Electronic absorption studies

Electronic absorption spectroscopy is normally used to investigate the binding of compounds with DNA [20, 21]. Absorption spectroscopic analysis was conducted by a spectrophotometer (Perkin Elmer Lambda-35) by using fixed concentrations of ligand or complex (50 µM) with increasing amounts of DNA in the range of 28.9 µM to 173.4 µM in a

6.3 mM Tris-HCl/50 mM NaCl buffer (pH 7). Each addition was left to stand at 25 °C for 10 min to reach equilibrium. The samples were then scanned from 230 nm to 600 nm. All ligands and their complexes revealed two absorption bands attributed to the transitions of π–π^* and n–π^* except for the **H_2L_4** ligand and its complex **[$MoO_2(L_4D)$]**, which only revealed the π–π^* transitions at 308 nm. The electronic absorption spectra of the complexes (Figs. 7 and 8) show the n–π^* transitions at 338 nm and the π–π^* transitions at 296, 304, and 306 nm for **[$MoO_2(L_1D)$]**, **[$MoO_2(L_2D)$]**, and **[$MoO_2(L_3D)$]**, respectively. The π–π^* absorption bands were utilized to observe the interaction of CT DNA with ligands and complexes. The changes in absorbance were characterized as hypochromism, which confirm that the complexes bind to the DNA through intercalation [22]. The values of these changes with increasing amounts of CT DNA were used to estimate the intrinsic binding constant K_b through the following equation [23]:

$$[DNA] / (\varepsilon_a - \varepsilon_f) = [DNA] / (\varepsilon_b - \varepsilon_f) + 1/K_b (\varepsilon_b - \varepsilon_f)$$

where the absorption coefficients ε_a, ε_f, and ε_b correspond to A_{abs}/[DNA], the extinction coefficient for the free complex, and the extinction coefficient for the complex in fully bound form, respectively. The plot of [DNA]/(ε_a- ε_f) versus [DNA] gives a slope 1/(ε_a – ε_f) and intercept 1/K_b (ε_b – ε_f) as shown in Fig. 9. The binding constants (Table 5) suggest that all ligands and complexes were bound to the CT DNA. The complexes revealed stronger interaction with the DNA compared with their ligands. The highest K_b values were recorded for **H_2L_3** and **[$MoO_2(L_3D)$]** (3.174×10^5 M^{-1} and 1.559×10^6 M^{-1}, respectively), whereas the lowest values were recorded for **H_2L_4** and **[$MoO_2(L_4D)$]** (1.342×10^4 M^{-1} and 1.00×10^5 M^{-1}), respectively. Furthermore, the binding of the complexes to CT DNA resulted in isosbestic spectral changes with an isosbestic point at 289 nm.

3.3.2. Fluorescence emission studies

Fluorescence spectroscopic analysis was conducted by a spectrophotometer (Jasco FP-750) at 25 °C in a 6.3 mM Tris-HCl/50 mM NaCl buffer (pH 7). Except for the complex **[$MoO_2(L_3D)$]**, the fluorescence spectra of all complexes (Figs. 10 and 11) show two emission bands at 380 and 500 nm. The changes in fluorescence intensity with increasing amounts of CT DNA were characterized as hypochromism at 500 nm and as hyperchromism at 380 nm. These changes can be attributed to the isosbestic spectral changes with an isosbestic point at 408 nm. The complex **[$MoO_2(L_3D)$]** revealed one emission band at 380 nm accompanied by a hypochromism in fluorescence emission intensity. These fluorescence emission intensities confirm the strong bound of the complexes to DNA.

3.3.3. Viscometric studies

Viscometric studies play an essential role in confirming the DNA binding pattern in the solution. The intercalation of a compound into DNA is known to increase viscosity because of the extension and stiffing of the DNA helix [24]. Viscometric analysis was performed by adding increasing amounts of the ligands and the complexes to CT DNA at 37 °C in a 6.3 mM Tris-HCl/50 mM NaCl buffer (pH 7). Results are presented in Fig. 12. In general, the addition of CT DNA results in an increase in the viscosity of the solutions of the complexes. These results confirm the intercalative binding and support the spectrometric results.

3.4. DNA cleavage studies

Agarose gel electrophoresis experiments with pBR322 circular plasmid DNA were performed to investigate the effect of various micro-concentrations (1.0µM to 6.0µM) of ligands and complexes on DNA cleavage. The assay was conducted in an aqueous buffer solution of 6.3 mM Tris-HCl/50 mM NaCl buffer (pH 7) with a fixed amount (4.5 µM) of

30% H_2O_2 serving as oxidant. The solution was incubated at 37 °C for 2 h. As shown in Figs. 13 and 14, lane 4 of the agarose gel electrophoresis reveals that **H_2L_1** and **H_2L_4** exhibit DNA cleavage in the plasmid DNA with typical two forms: the fast migration form related to the closed circular supercoiled form (SC, form I) and the slow migration form related to the open circular relaxed form (OC, form II) [25]. **H_2L_2** and **H_2L_3** can niked both strands of the plasmid DNA, consequently showing the linear form (form III) at a concentration of 5 µM (lane 10) accompanied by the disappearance of the second form (OC, form II) when the concentration increases to 6 µM (lane 11) Thus, **H_2L_2** exhibits all three forms of plasmid DNA, whereas the other ligands show the inhibition of migration of the plasmid DNA at this concentration.

The complexes exhibited SC form I, OC form II, and linear form III. For the complex **[$MoO_2(L_1D)$]**, forms I and III were exhibited at a concentration of 4 µM. However, form I disappeared and form II reappeared with form III (lane 9) when the concentration increased to 4.5 µM. When the concentration further increased to 5 µM, only form III remained (lane 10). For the complex **[$MoO_2(L_2D)$]**, forms I and III were exhibited at a concentration of 4.5 µM (lane 9). When the concentration increased to 5 µM, form I disappeared and only form III remained (lane 10). Given that the complex **[$MoO_2(L_3D)$]** can niked both strands of the plasmid DNA, forms I and III were exhibited at a concentration of 3 µM (lane 6). When the concentration increased to 3.5 µM, all three forms were exhibited (lane 7). The complex **[$MoO_2(L_4D)$]** exhibited forms II and III at a concentration of 4.5 µM (lane 9) and only form II at a concentration of 5 µM (lane 10). The inhibitory action of the complexes on the plasmid DNA were demonstrated at a concentration of 6 µM for **[$MoO_2(L_1D)$]**, **[$MoO_2(L_2D)$]**, and **[$MoO_2(L_4D)$]** and at a concentration of 4 µM for **[$MoO_2(L_3D)$]**. On the basis of the size fragments of the ladder DNA (lane L), the size of form II increased as the concentrations of **[$MoO_2(L_1D)$]**, **[$MoO_2(L_2D)$]**, and **[$MoO_2(L_4D)$]** increased, which are consistent with their

respective ligands **H_2L_1**, **H_2L_2**, and **H_2L_4**. However, the complex **[$MoO_2(L_3D)$]** exhibited a different behavior from the other complexes. The size of form II decreased as the concentrations increased, which is inconsistent with the behavior of its respective ligand **H_2L_3**. The agarose gel electrophoresis patterns show only the naturally occurring supercoiled form (SC, form I) for DNA control and buffer (lane 1), DNA and ligand or complexes (lane 2), and DNA, H_2O_2, and buffer (lane 3). This finding indicates that the activity of ligands and complexes to cleave DNA can only be accomplished in the presence of H_2O_2 acting as oxidant (lanes 4–11) by adding a fixed amount (4.5 μM) of H_2O_2 to different amounts of ligands and complexes (1 μM to 6 μM).

The activity to cleave DNA was greatly enhanced in complexes compared with their related free ligands, which proves that the complexes can produce hydroxyl radical from H_2O_2. This capability to generate hydroxyl radicals from metal ions is well reported [26, 27]. These free radicals share the oxidation of deoxyribose moiety, followed by the hydrolytic cleavage activity of the sugar phosphate backbone [28].

3.5. Antitumor activity

Similar to the DNA binding and the DNA cleavage activity, the complexes demonstrated higher efficiency in anti-proliferation activity compared with their respective ligands. Anti-proliferation tests of the complexes against HCT 116 cancer cells were performed *in vitro*. The complexes exhibited greater pronounced activity than the standard reference 5-fluorouracil did (IC_{50} = 7.3 μM). The median inhibitory concentrations (IC_{50}) of the tested compounds are presented in Table 6. Results show that the anti-proliferative efficiency of the complexes are in the following order: **[$MoO_2(L_3D)$] > [$MoO_2(L_1D)$] ~ [$MoO_2(L_2D)$] > [$MoO_2(L_4D)$]**. These results justify the importance of substituents in the aromatic ring on anti-proliferation efficiency, which are in the following order: $C(CH_3)_3$ > Cl

~ CH_3 > OH. These results are consistent with the binding capabilities of the complexes with CT DNA. The presence of the terminal N-ethyl and tert-butyl groups provide strong lipophilic properties that enable the complex **[$MoO_2(L_3D)$]** to move into the hydrophobic medium of DNA. The terminal N-methyl and N-ethyl groups as well as the chlorine and methyl moieties, are provide good lipophilic properties that enable the complex **[$MoO_2(L_1D)$]** and **[$MoO_2(L_2D)$]** to move into DNA, respectively. The polarized chlorine moiety increases the London dispersion forces, which are well increase the lipophilic properties of **[$MoO_2(L_1D)$]**. The presence of hydroxyl group adjacent to O(1) in **[$MoO_2(L_4D)$]** can form a strong intrahydrogen bonds between them, which decreases the lipophilic properties while increasing the hydrophilic properties, consequently decreasing its efficiency to move between the DNA bases. Meanwhile, the coordination with MoO_2^{+2} unit leads to geometrical and conformational changes which in turn lead to an extent of planarity which increases the affinity between the complexes and DNA, consequently leads to increases the apoptosis ability of complexes against the cell proliferation. Furthermore, the inhibition activity of complexes showed that 100 µM of **[$MoO_2(L_3D)$]**, **[$MoO_2(L_1D)$]**, **[$MoO_2(L_2D)$]**, and **[$MoO_2(L_4D)$]** is sufficient to inhibit 95.6%, 91.3%, 76.9%, and 48.9% of cell proliferation, respectively (Fig. 15). Figure 16 shows the photomicrographs of HCT 116 cell images after 48 h treatment with the complexes. These images were taken under an inverted phase-contrast microscope at ×200 magnification with a digital camera after 48 h of treatment with the samples. The photomicrograph of the untreated (control) group showed aggressively growing cells with full confluence and compact monolayer of HCT 116 cells. A closer examination of the images of untreated and treated cells reveals the strong cytotoxic effect of the complexes against the HCT 116 cell line. The analysis of the photomicrographs shows that the complexes generally show apoptotic features in the affected cells. The blabbing of the cell membrane, the nuclear

condensation, and the formation of vesicles in the treated cells clearly indicate the unique characteristics of apoptosis.

4. Conclusions

The synthetic and structural descriptions, as well as the biological evaluation, of four molybdenum(VI) complexes (**[$MoO_2(L_1D)$]–[$MoO_2(L_4D)$]**) were studied. The complexes show that the thiosemicarbazonato ligands (**L_1–L_4**) of *N*-methyl-2-(5-chloro-2-hydroxybenzylidene) hydrazinecarbothioamide (**H_2L_1**), *N*-ethyl-2-(5-methyl-2-hydroxybenzylidene) hydrazinecarbothioamide (**H_2L_2**), *N*-ethyl-2-(3-ter-butyl-2-hydroxybenzylidene) hydrazinecarbothioamide (**H_2L_3**), and *N*-methyl-2-(2,3-dihydroxylbenzylidene) hydrazinecarbothioamide (**H_2L_4**) are coordinated to molybdenum as tridentate ONS-donors. On the basis of the X-ray crystallography results, all complexes show the distorted octahedral coordination. The complexes reveal good efficiency for CT DNA binding, which is supported by the high values of the binding constant K_b in the range 1.00×10^5 M^{-1} to 1.559×10^6 M^{-1}, the UV hypochromism of the absorption bands at 296 and 305 nm, the increase in viscosity with increasing CT DNA concentrations, and the efficient cleavage activity of the plasmid pBR322 DNA. The complexes exhibit higher activity compared with their respective ligands.

The anti-proliferative activities of the complexes against HCT 116 cell lines were investigated. All complexes exhibit high *in vitro* anticancer activities in the relative order **[$MoO_2(L_3D)$] > [$MoO_2(L_1D)$] ~ [$MoO_2(L_2D)$] > [$MoO_2(L_4D)$]** according to their IC_{50} values of 3.2, 4.5, 4.6, and 6.4 μM, respectively.

Acknowledgements

We thank the Malaysian Government for a Research University Grant which partly supported this work . We also thank University of Basrah, Iraq, for the study leave to Mouayed A. Hussein.

Supplementary material

CCDC 931643 and 925646 contain the supplementary data for $\mathbf{H_2L_2}$ and $\mathbf{H_2L_3}$. CCDC 891975, 902962, 902960, and 906634 contain the supplementary data for **[$MoO_2(L_1D)$]–[$MoO_2(L_4D)$],** respectively. These data can be obtained free of charge from http://www.ccdc.cam.ac.uk/data_request/cif.

References

[1] M. Belicchi Ferrari, F. Bisceglie, G. Pelosi, P. Tarasconi, R. Albertini, P.P. Dall Aglio, S Pinelli, A. Bergamo, G. Sava, J.Inorg. Biochem. 98(2004) 301.

[2] Z. Afrasiabi, E. Sinn, J. Chen, Y. Ma, A.L. Rheingold, L.N. Zakharov, N. Rath, S. Padhye, Inorg. Chim. Acta 357(2004) 271.

[3] H. Beraldo, D. Gambino, Mini Rev. Med. Chem. 4(2004) 31.

[4] S.I.Pascu, P.A. Waghorn, T.D. Corny, B. Lin, H.M. Betts, J.R. Dilworth, R.B. Sim, G. C. Churchill, F. I. Aigbirhio, J.E. Warren, Dalton Trans 16(2008) 2107.

[5] J. Yuan, D.B. Lovejoy, D.R. Richardson, Blood 55(2000) 937.

[6] R. R. Mrndel, F. Bittner, Biochim. Biophys. Acta Mol. Cell Res 1763 (2006) 621.

[7] C. D. Brondino, M. J. Romao, I. Moura, J.J.G. Moura, Curr. Opin. Chem.Biol. 10 (2006) 109.

[8] G. D'Errico, A. D. Salle, F. L. Cara, M. Rossi, R. Cannio, J. Bacteriol. 188 (2006) 694.

[9] R. Harrison, Free Radic. Biol. Med. 33 (2002) 774.

[10] D.C. Pryde, J. Med. Chem. 53 (2010) 8441.

[11] R. Dinda, P. Sengupta, S. Ghosh, H. Mayar-Figge, W.S. Sheldrick, J. Chem. Soc., Dalton Trans. (2002) 4434.

[12] N. K. Ngan, K.M. Lo, C.S.R. Wong, Polyhedron 33 (2012) 235.

[13] S. Quintal, J. Matos, I. Fonseca, V. Félix, Drew, M.G.B. Drew, N. Trindade, M. Meireles, M.J. Calhorda, Inorg. Chim. Acta 361(2008) 1584.

[14] E.B. Seena, M.R. Prathapachandra Kurup, Polyhedron 26(2007) 3595.

[15] V. Vrdoljak, I. Dilovic, M. Rubcic, S. Kraljevic Pavelic, M. Kralj, D. Matkovic-Calogovic, I. Piantanida, P. Novak, A. Rozman, M. Cindric, Eur. J. Med. Chem. 45 (2010) 38.

[16] G.M. Sheldrick, Acta Cryst. A64 (2008) 112.

[17] D. Eierhoff, W. C. Tung, A. Hammerschmidt, B. Krebs ,Inorg. Chimi. Acta 362 (2009) 915.

[18] C. Icsel, V.T. Yilmas, F. Ari, E. Ulukaya, W.T.A. Harrison, Eur. J. Med. Chem. 60 (2013) 386.

[19] T. Mosmann, J. Immunol. Methods 65 (1983) 55.

[20] T.S. Kamatchi, N. Chitrapriya, S.K. Kim, F.R. Fronczek, K. Natarajan, Eur. J. Med. Chem. 59(2013) 253.

[21] S. Tabassum, M. Zaki, F. Arjmand, I. Ahmad, Photochem. Photobiol. B 114(2012) 108.

[22] S.K. Thangavel, C. Nataraj, K.K. Seog, R.F. Frank and N. Karuppannan, Eur. J. Med. Chem. 59(2013) 253-264.

[23] A. Wolfe, G.H. Shimer, T. Meehan, 26(1987) 6392.

[24] S. Satyanarayana, J.C. Dabrowiak, J.B. Chaires, Biochemistry 31 (1992) 9319.

[25] E.J. Gao, M.C. Zhu, Y. Huang, L. Liu, F.C. Liu, S. Ma, C.Y. Shi, Eur. J. Med. Chem. 45(2010) 1034.

[26] A.D. Richards, A. Rodgers, Chem. Soc. Rev. 36 (2007) 471.

[27] F.R. Liu, K.Z. Wang, G.Y Bai, Y.A. Zhang, L.H. Gao, Inorg Chem. 43 (2004) 1799.

[28] C. X. Zhang, S. J. Lippard, Curr. Op. Chem. Biol. 7 (2003) 481.

Graphical abstract

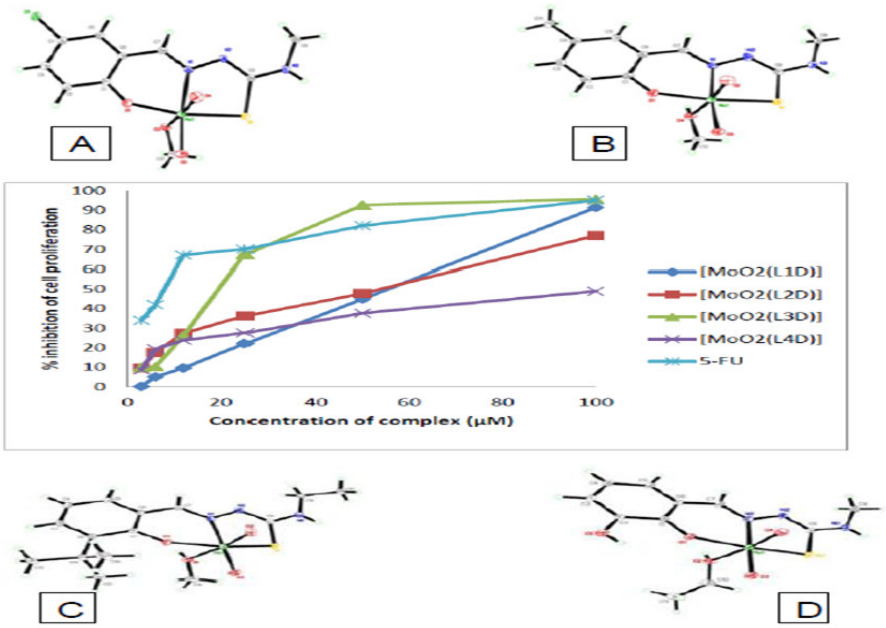

Percentage of cell proliferation inhibition by A= [MoO_2(L_1 D)] , B= [MoO_2(L_2 D)], C= [MoO_2(L_3 D)] and D=[MoO_2(L_4 D)].

Figure captions

Scheme 1. General synthetic procedure of ligands and complexes

Fig 1. Molecular structure of $\mathbf{H_2L_2}$

Fig 2. Molecular structure of $\mathbf{H_2L_3}$

Fig 3. Molecular structure of $\mathbf{[MoO_2(L_1D)]}$

Fig 4. Molecular structure of $\mathbf{[MoO_2(L_2D)]}$

Fig 5. Molecular structure of $\mathbf{[MoO_2(L_3D)]}$

Fig 6. Molecular structure of $\mathbf{[MoO_2(L_4D)]}$

Fig. 7. UV spectra of complexes $\mathbf{[MoO_2(L_1D)]}$ and $\mathbf{[MoO_2(L_2D)]}$ in 6.3 mM Tris-HCl/50 mM NaCl buffer (pH= 7) in presence of CT DNA at increasing amounts.[complex] = 50 µM , [DNA] = (28.9 - 173.4) µM . The arrows show the changes in absorbance upon increasing amounts of CT - DNA .

Fig. 8. UV spectra of complexes $\mathbf{[MoO_2(L_3D)]}$ and $\mathbf{[MoO_2(L_4D)]}$ in 6.3 mM Tris-HCl/50 mM NaCl buffer (pH= 7) in presence of CT DNA at increasing amounts.[complex] = 50 µM , [DNA] = (28.9 - 173.4) µM . The arrows show the changes in absorbance upon increasing amounts of CT-DNA .

Fig. 9. Plots of $[DNA]/(\varepsilon_a - \varepsilon_f)$ vs [DNA] for A= $\mathbf{[MoO_2(L_1D)]}$, B= $\mathbf{[MoO_2(L_2D)]}$, C= $\mathbf{[MoO_2(L_3D)]}$ and D= $\mathbf{[MoO_2(L_4D)]}$.

Fig. 10. Fluorescence spectra of complexes $\mathbf{[MoO_2(L_1D)]}$ and $\mathbf{[MoO_2(L_2D)]}$ in 6.3 mM Tris-HCl/50 mM NaCl buffer (pH= 7) in presence of CT - DNA at increasing

amounts.[complex] = 50 μM , [DNA] = (28.9 - 173.4) μM. The arrows show the changes in fluorescence intensity upon increasing amounts of CT - DNA.

Fig. 11. Fluorescence spectra of complexes **[$MoO_2(L_3D)$]** and **[$MoO_2(L_4D)$]** in 6.3 mM Tris-HCl/50 mM NaCl buffer (pH= 7) in presence of CT DNA at increasing amounts.[complex] = 50 μM , [DNA] = (28.9 - 173.4) μM. The arrows show the changes in fluorescence intensity upon increasing amounts of CT - DNA.

Fig. 12. Viscometric results of ligands (A) and complexes (B) , in 6.3 mM Tris-HCl/50 mM NaCl buffer (pH= 7) upon addition increasing amounts of CT DNA.

Fig. 13. Agarose gel electrophoresis patterns of pBR 322 (0.025 μM) increasing concentrations (1.0 μM – 6.0 μM) of ligands **H_2L_1** and **H_2L_2** and their complexes **[$MoO_2(L_1D)$]** and **[$MoO_2(L_2D)$]** in 6.3 mM Tris-HCl/50 mM NaCl buffer (pH= 7) incubated at 37 ^{0}C for 2h , using H_2O_2 (4.5 μM) and ladder 1 KbDNA as a marker (lane L); lane 1, pBR 322 DNA ; lane 2, DNA + Sample (ligand or complex)(6 μM); lane 3, DNA+ H_2O_2 ; lane 4, DNA +H_2O_2+ Sample (1 μM);lane 5, DNA +H_2O_2+ Sample(2 μM); lane 6, DNA +H_2O_2+ Sample (3 μM); lane 7 , DNA +H_2O_2+ Sample(3.5 μM); lane 8, DNA +H_2O_2+ Sample(4 μM); lane 9, DNA +H_2O_2+ Sample(4.5 μM); lane 10, DNA +H_2O_2+ Sample (5 μM); lane 11, DNA +H_2O_2+ Sample(6 μM).

Fig. 14. Agarose gel electrophoresis patterns of pBR 322 (0.025 μM) increasing concentrations (1.0 μM – 6.0 μM) of ligands **H_2L_3** and **H_2L_4** and their complexes **[$MoO_2(L_3D)$]** and **[$MoO_2(L_4D)$]**.

Fig. 15. Cell proliferation inhibition by complexes in concentration range 3.0-100 μM using 5-FU as a reference.

Fig. 16. Photomicrographs of the HCT 116 cell lines before and after treatment with complexes ; image control = HCT 116 cell before treatment , the images after treatment ; A=**[$MoO_2(L_1D)$]** (IC_{50}=4.5 µM), B=**[$MoO_2(L_2D)$]** (IC_{50}=4.6 µM), C=**[$MoO_2(L_3D)$]** (IC_{50}=3.2 µM), D=**[$MoO_2(L_4D)$]** (IC_{50}=6.4 µM) and 5-FU= standard reference (IC_{50}=7.3 µM) .

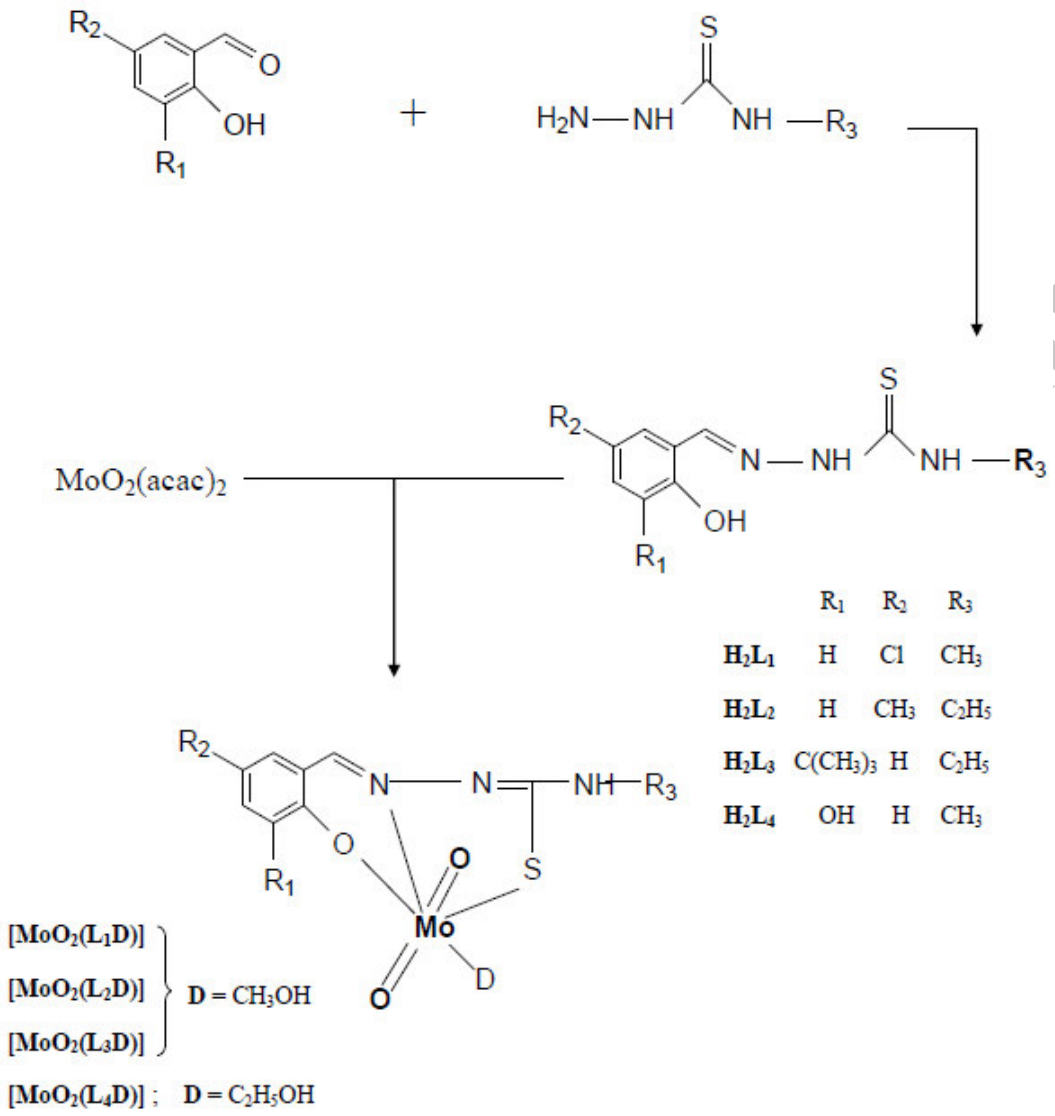

Scheme 1. General synthetic procedure of ligands and complexes

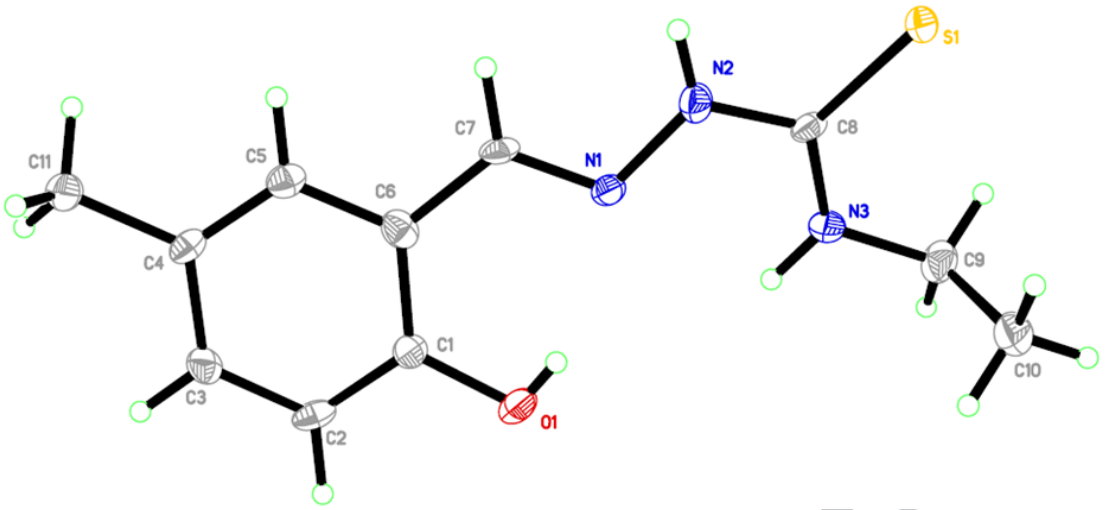

Fig 1. Molecular structure of H_2L_2

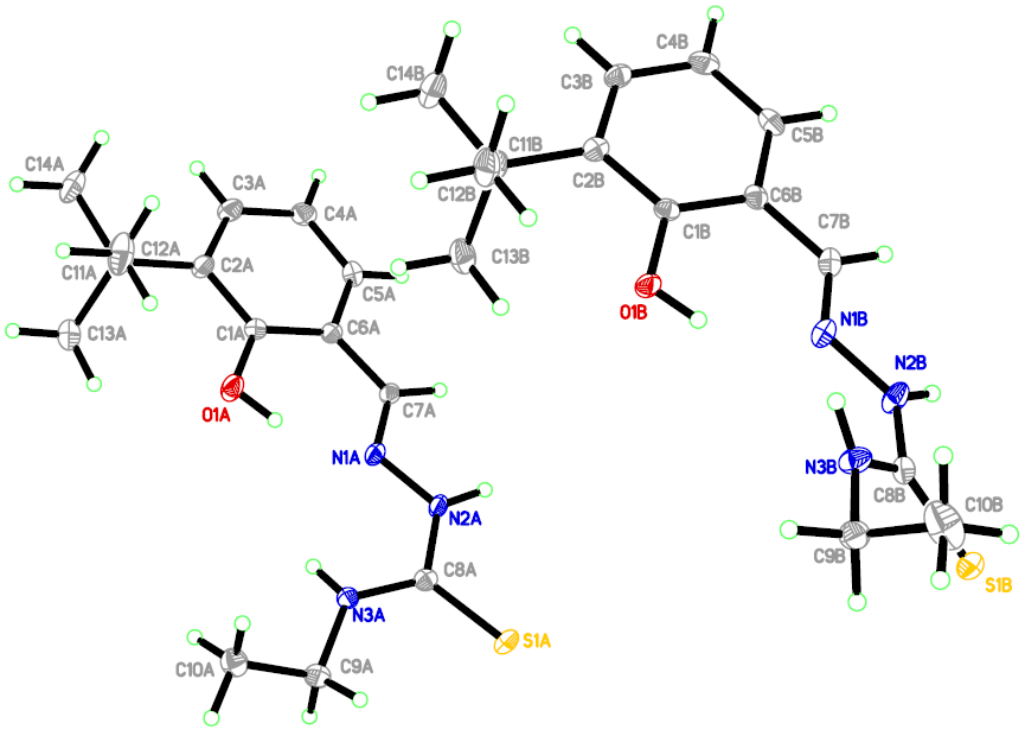

Fig 2. Molecular structure of H_2L_3 (A and B)

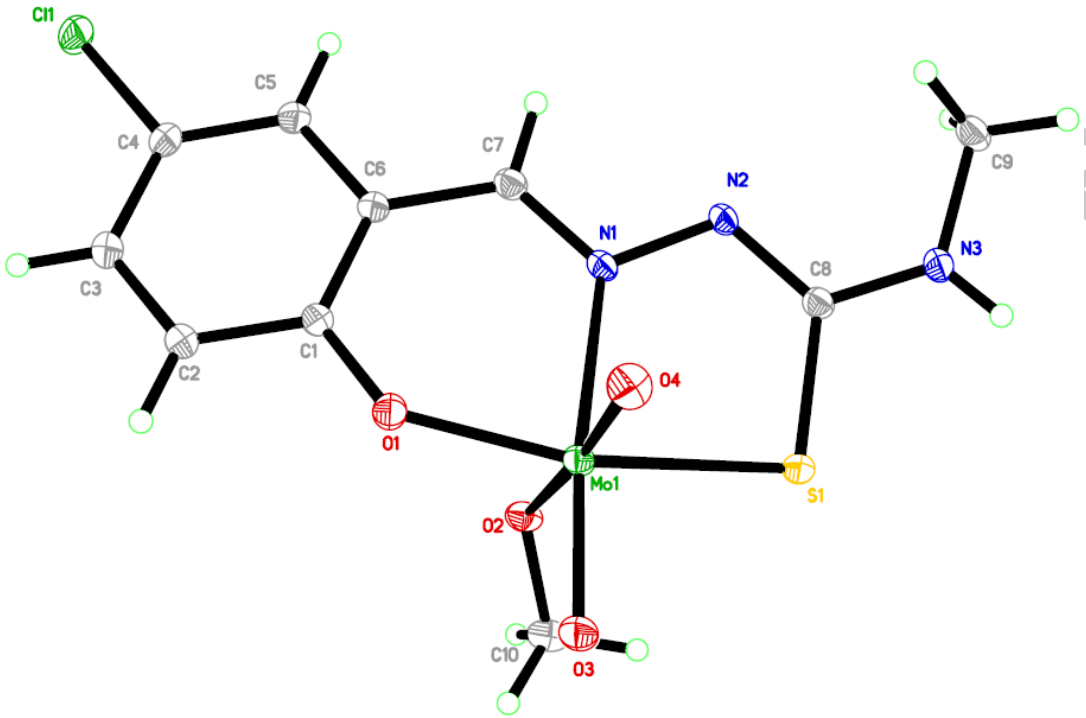

Fig 3. Molecular structure of **[$MoO_2(L_1D)$]**

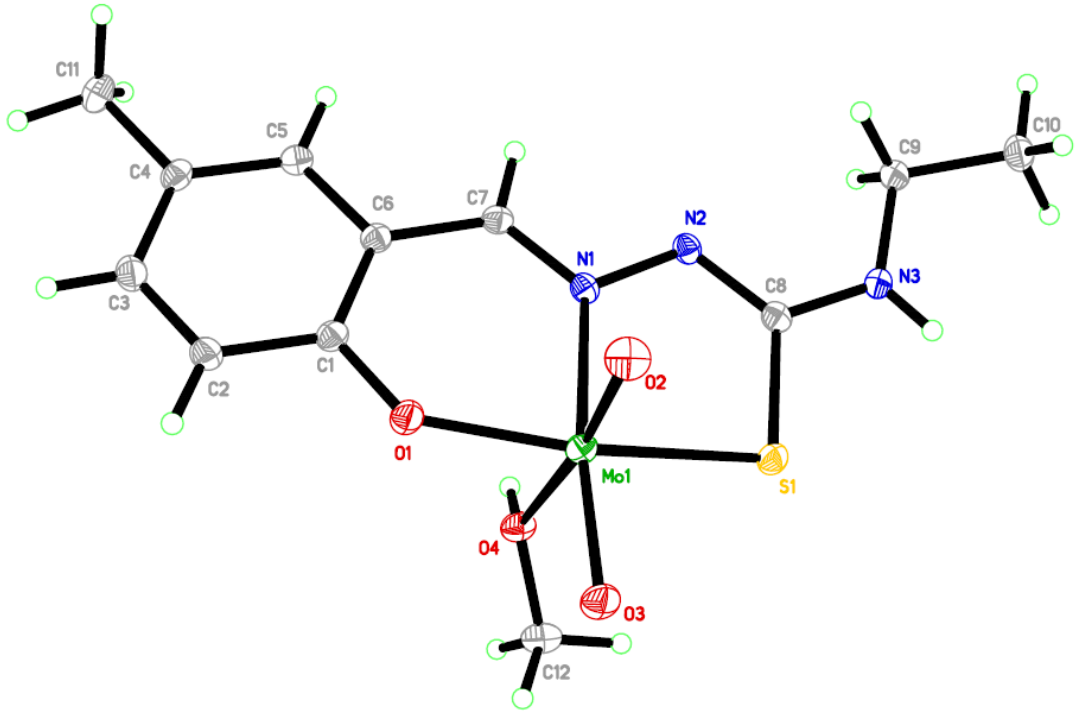

Fig 4. Molecular structure of **[$MoO_2(L_2D)$]**

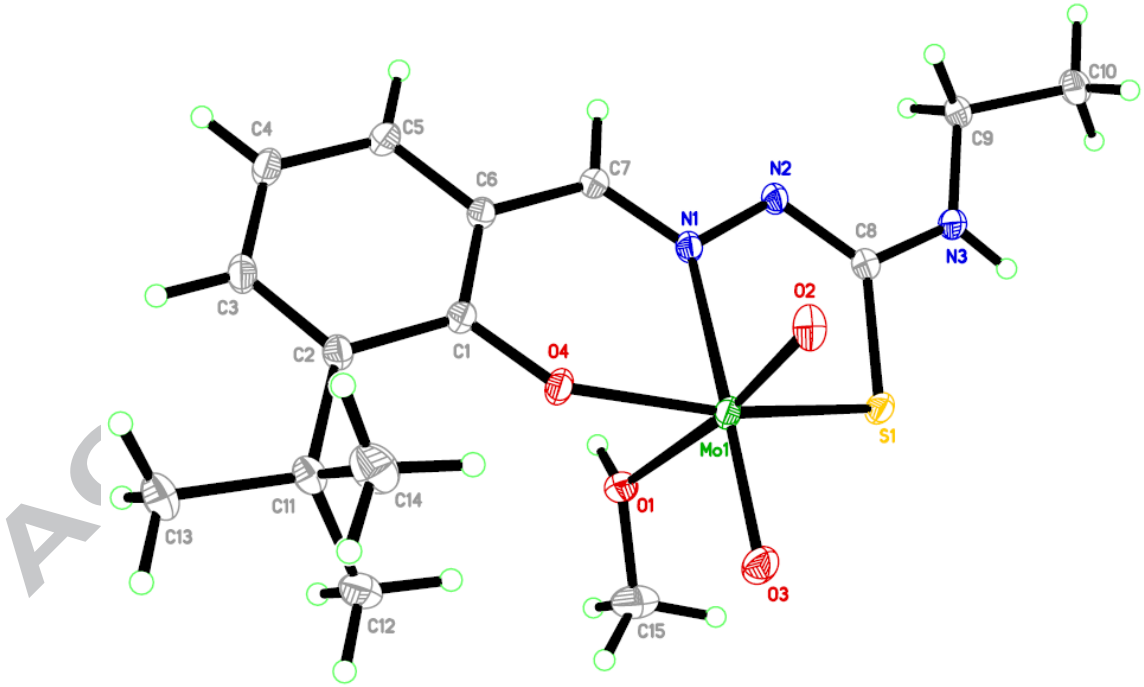

Fig 5. Molecular structure of **[$MoO_2(L_3D)$]**

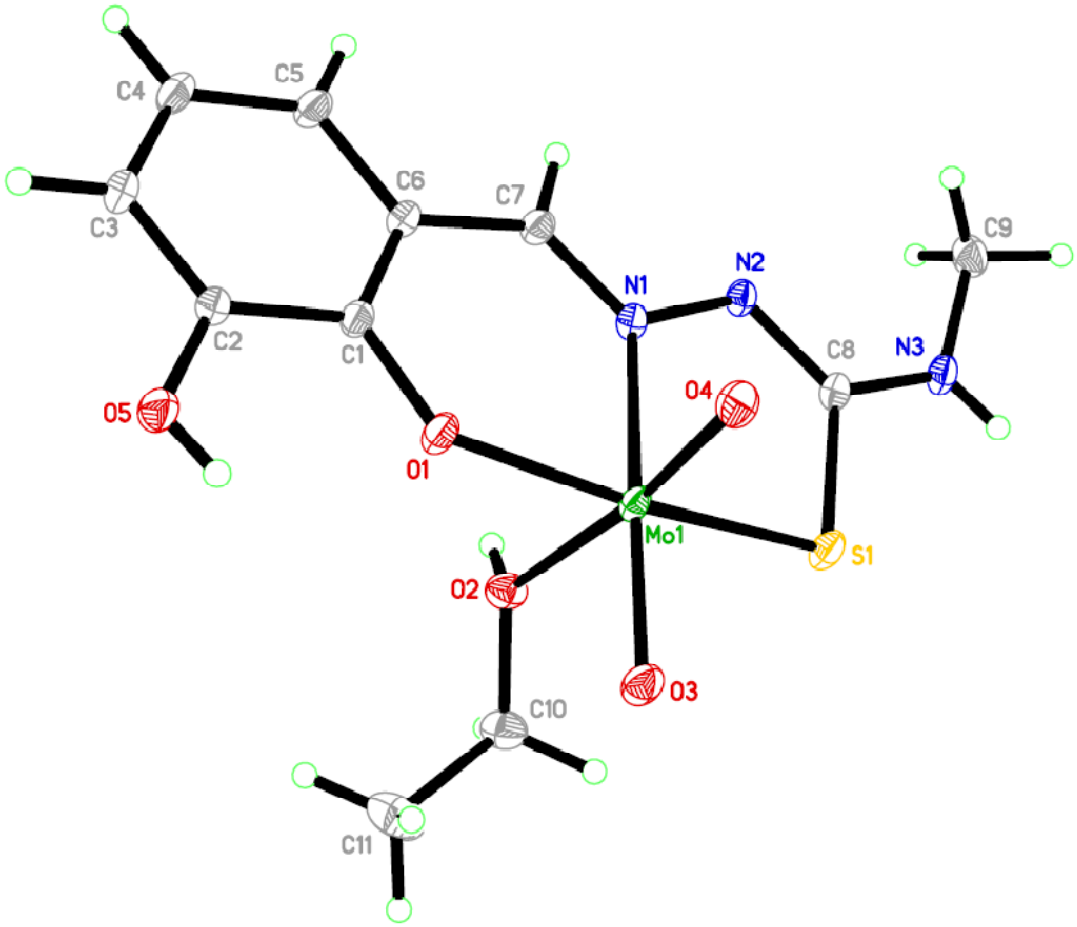

Fig 6. Molecular structure of **[$MoO_2(L_4D)$]**

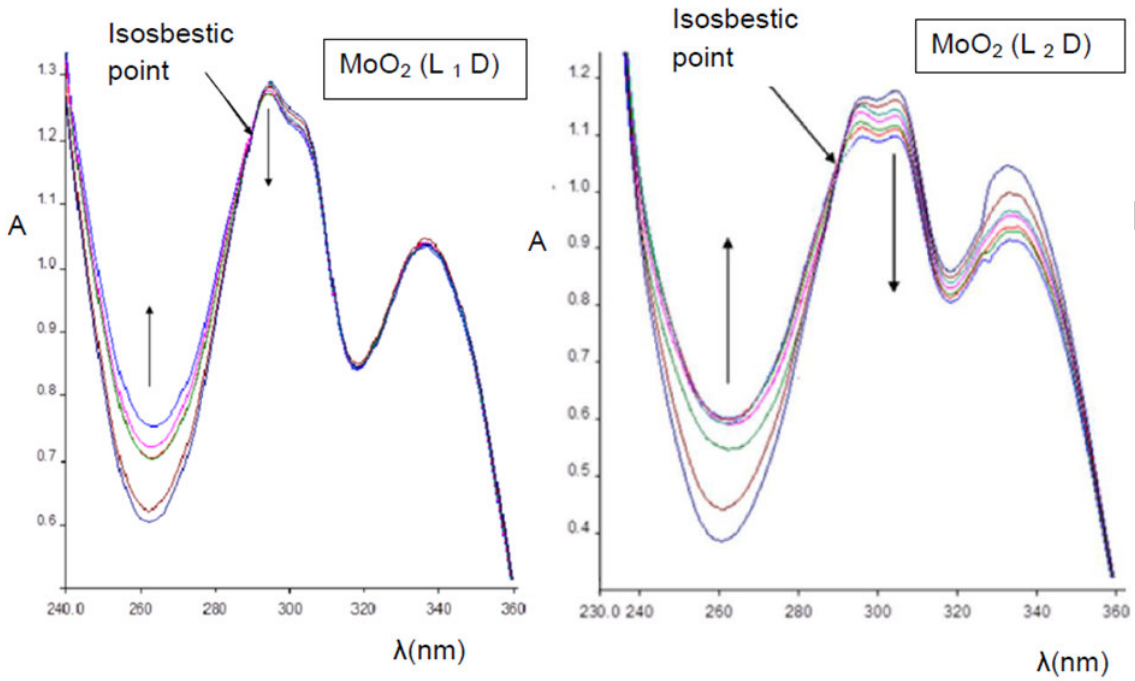

Fig. 7. UV spectra of complexes **[$MoO_2(L_1D)$]** and **[$MoO_2(L_2D)$]** in 6.3 mM Tris-HCl/50 mM NaCl buffer (pH= 7) in presence of CT DNA at increasing amounts.[complex] = 50 µM , [DNA] = (28.9 - 173.4) µM . The arrows show the changes in absorbance upon increasing amounts of CT - DNA .

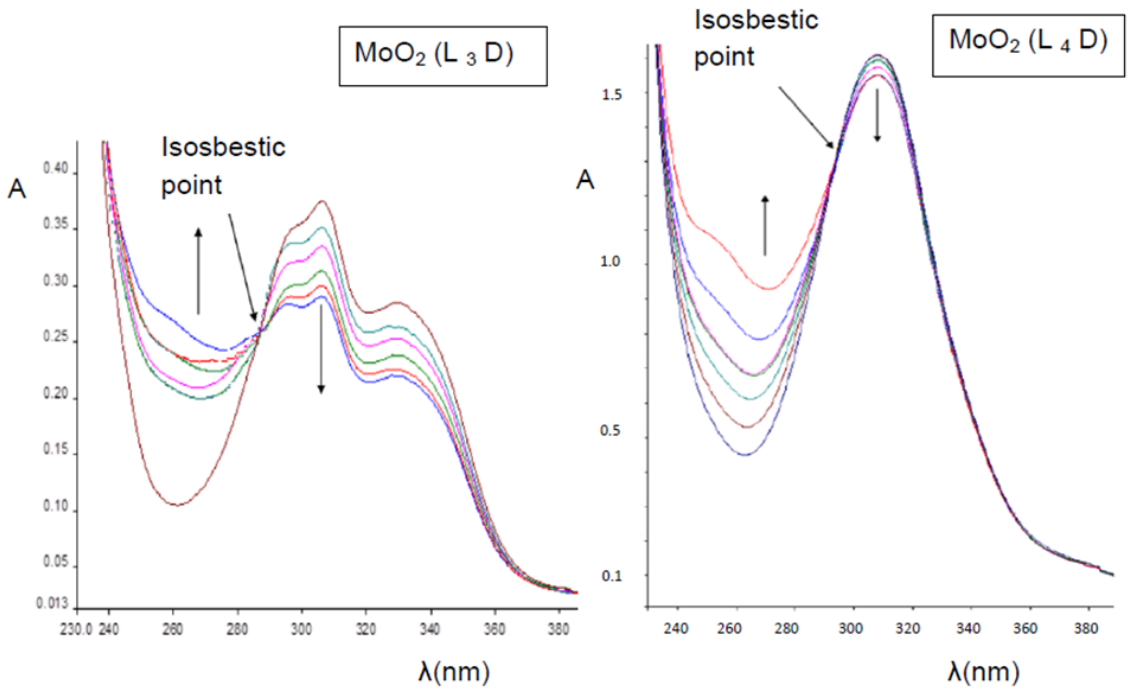

Fig. 8. UV spectra of complexes **[$MoO_2(L_3D)$]** and **[$MoO_2(L_4D)$]** in 6.3 mM Tris-HCl/50 mM NaCl buffer (pH= 7) in presence of CT DNA at increasing amounts.[complex] = 50 µM , [DNA] = (28.9 - 173.4) µM . The arrows show the changes in absorbance upon increasing amounts of CT-DNA .

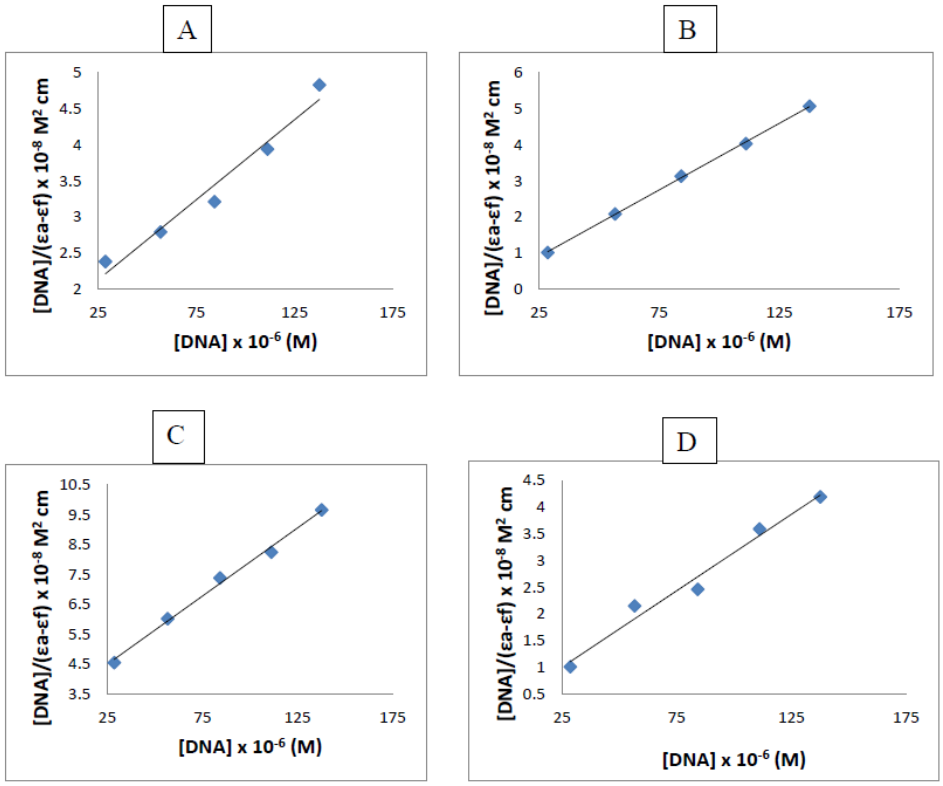

Fig. 9. Plots of [DNA]/(ε_a – ε_f) vs [DNA] for A= **[$MoO_2(L_1D)$]**, B= **[$MoO_2(L_2D)$]**, C= **[$MoO_2(L_3D)$]** and D= **[$MoO_2(L_4D)$]**.

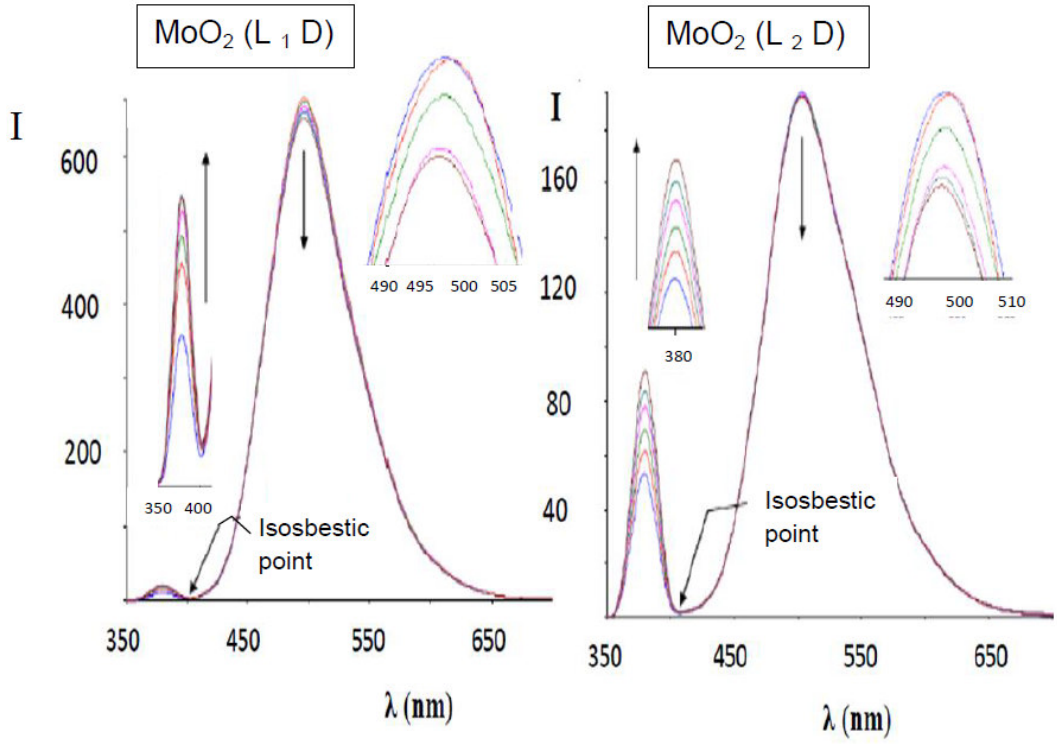

Fig. 10. Fluorescence spectra of complexes **[$MoO_2(L_1D)$]** and **[$MoO_2(L_2D)$]** in 6.3 mM Tris-HCl/50 mM NaCl buffer (pH= 7) in presence of CT - DNA at increasing amounts.[complex] = 50 µM , [DNA] = (28.9 - 173.4) µM. The arrows show the changes in fluorescence intensity upon increasing amounts of CT - DNA.

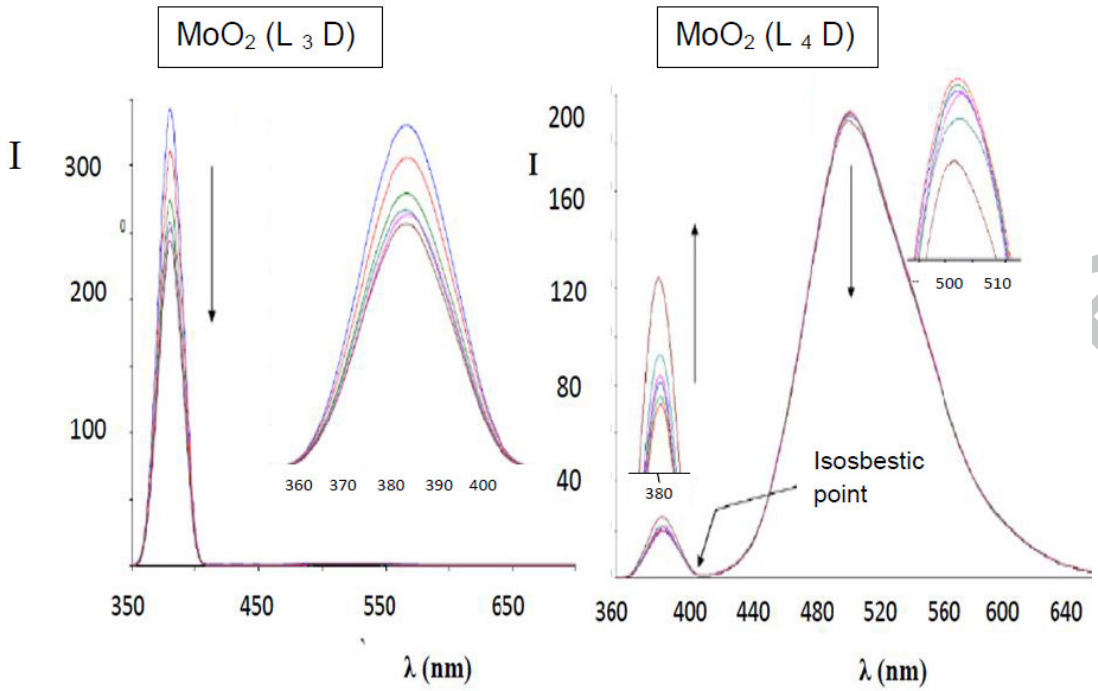

Fig. 11. Fluorescence spectra of complexes **[$MoO_2(L_3D)$]** and **[$MoO_2(L_4D)$]** in 6.3 mM Tris-HCl/50 mM NaCl buffer (pH= 7) in presence of CT DNA at increasing amounts.[complex] = 50 µM , [DNA] = (28.9 - 173.4) µM. The arrows show the changes in fluorescence intensity upon increasing amounts of CT - DNA.

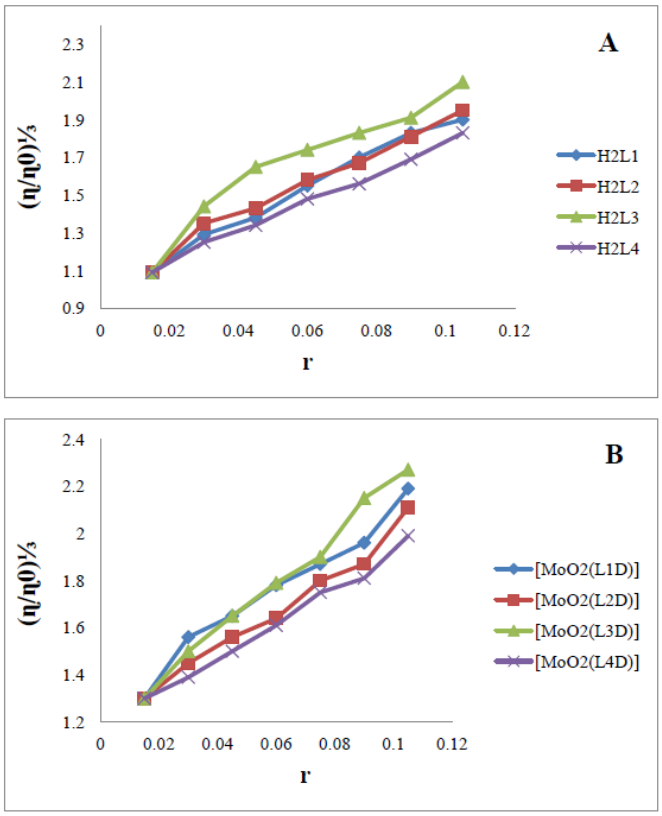

Fig. 12. Viscometric results of ligands (A) and complexes (B) , in 6.3 mM Tris-HCl/50 mM NaCl buffer (pH= 7) upon addition increasing amounts of CT DNA.

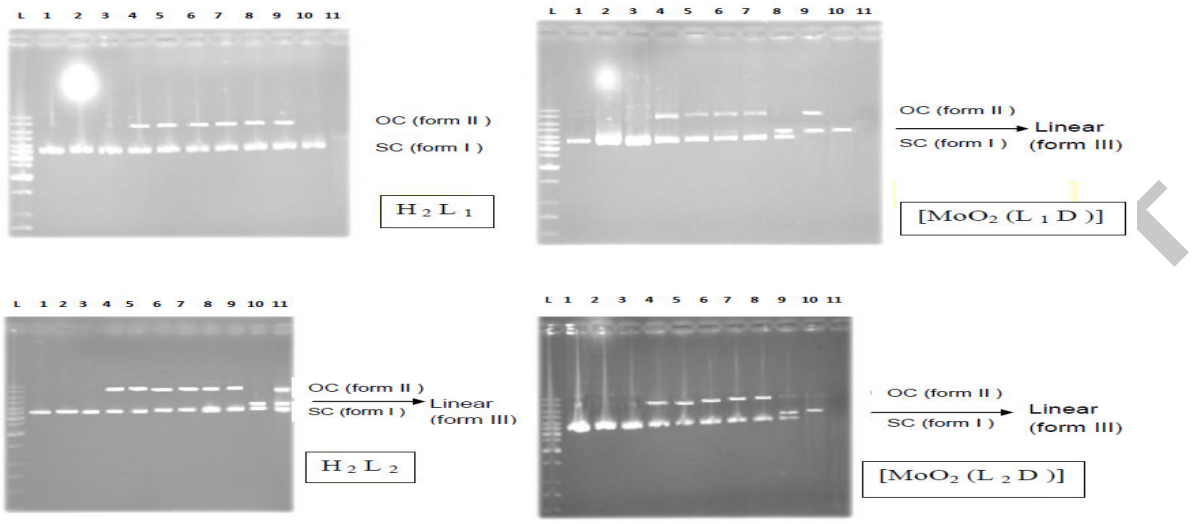

Fig. 13. Agarose gel electrophoresis patterns of pBR 322 (0.025 µM) increasing concentrations (1.0 µM – 6.0 µM) of ligands **H_2L_1** and **H_2L_2** and their complexes **[$MoO_2(L_1D)$]** and **[$MoO_2(L_2D)$]** in 6.3 mM Tris-HCl/50 mM NaCl buffer (pH= 7) incubated at 37 ^{0}C for 2h , using H_2O_2 (4.5 µM) and ladder 1 KbDNA as a marker (lane L); lane 1, pBR 322 DNA ; lane 2, DNA + Sample (ligand or complex)(6 µM); lane 3, DNA+ H_2O_2 ; lane 4, DNA +H_2O_2+ Sample (1 µM);lane 5, DNA +H_2O_2+ Sample(2 µM); lane 6, DNA +H_2O_2+ Sample (3 µM); lane 7 , DNA +H_2O_2+ Sample(3.5 µM); lane 8, DNA +H_2O_2+ Sample(4 µM); lane 9, DNA +H_2O_2+ Sample(4.5 µM); lane 10, DNA +H_2O_2+ Sample (5 µM); lane 11, DNA +H_2O_2+ Sample(6 µM).

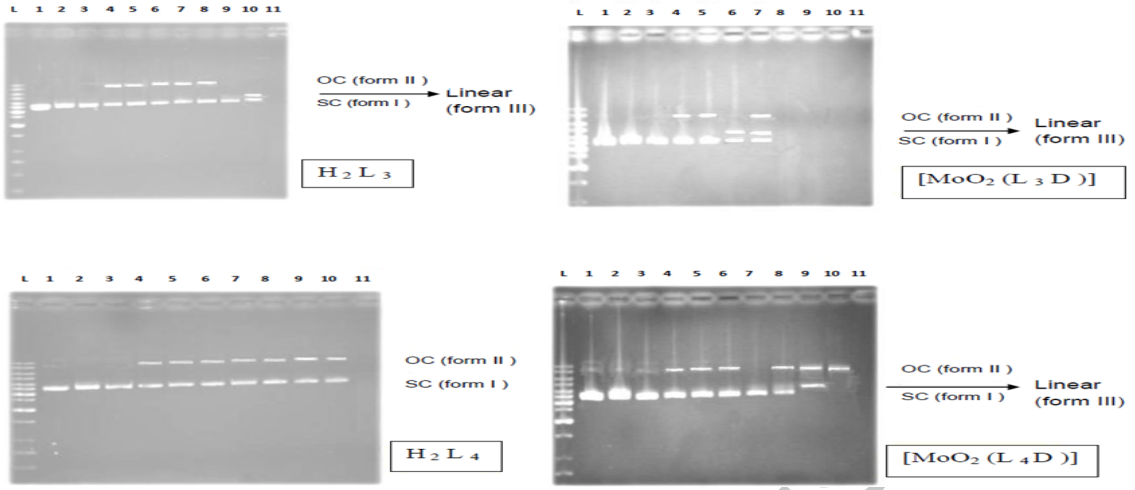

Fig. 14. Agarose gel electrophoresis patterns of pBR 322 (0.025 µM) increasing concentrations (1.0 µM – 6.0 µM) of ligands **H_2L_3** and **H_2L_4** and their complexes **[$MoO_2(L_3D)$]** and **[$MoO_2(L_4D)$]** in 6.3 mM Tris-HCl/50 mM NaCl buffer (pH= 7).

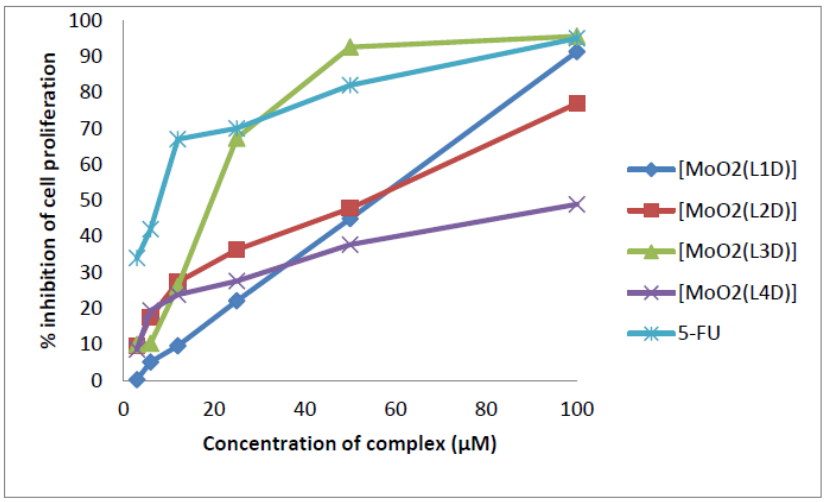

Fig. 15. Cell proliferation inhibition by complexes in concentration range 3.0-100 µM using 5-FU as a reference.

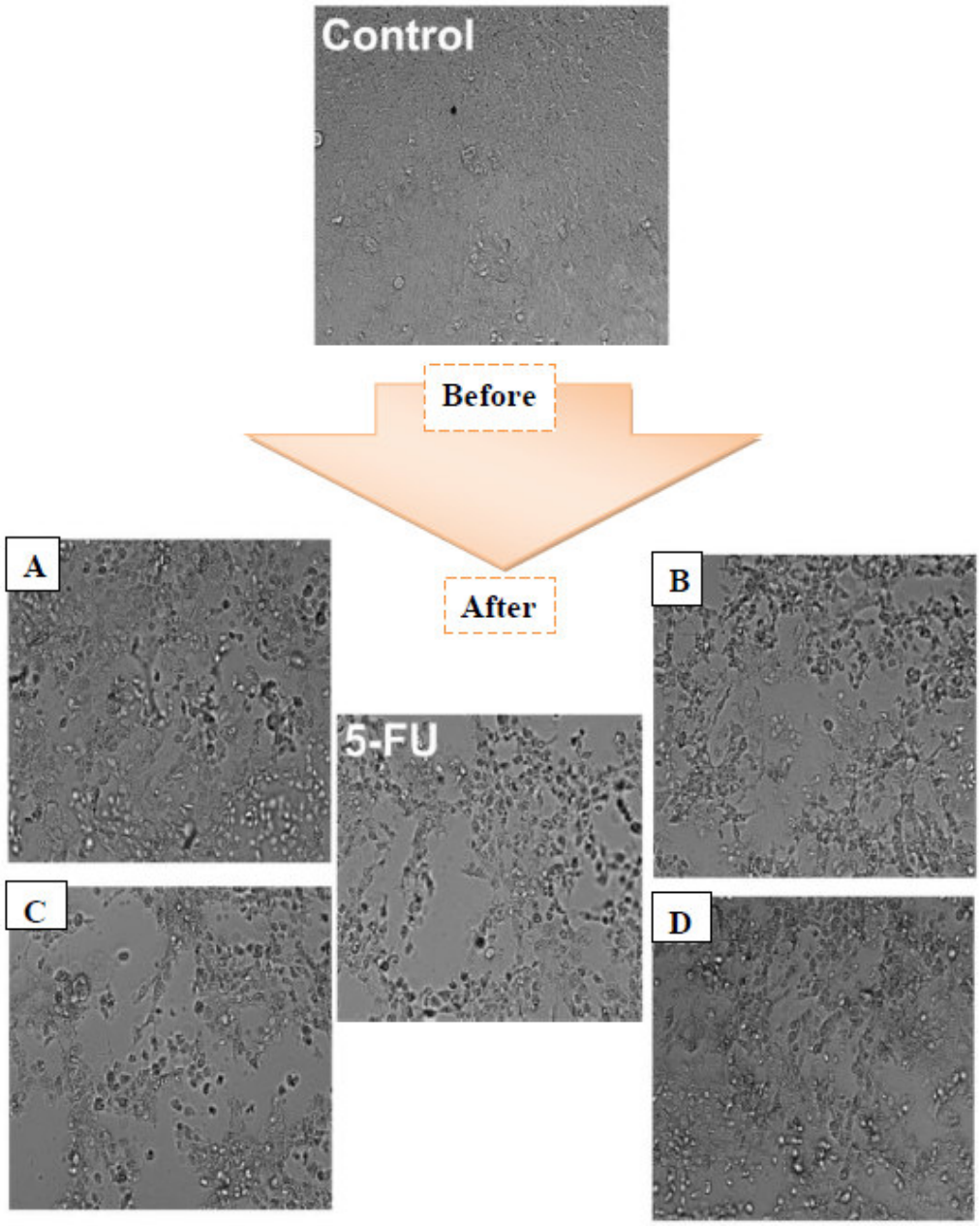

Fig. 16. Photomicrographs of the HCT 116 cell lines before and after treatment with complexes ; image control = HCT 116 cell before treatment , the images after treatment ; A=**[$MoO_2(L_1D)$]** (IC_{50}=4.5 µM) , B=**[$MoO_2(L_2D)$]** (IC_{50}=4.6 µM) , C=**[$MoO_2(L_3D)$]** (IC_{50}=3.2 µM) , D=**[$MoO_2(L_4D)$]** (IC_{50}=6.4 µM) and 5-FU= standard reference (IC_{50}=7.3 µM).

Table captions

Table 1

Crystallographic data for ligands **H_2L_2** and **H_2L_3**

Table 2

Crystallographic data for complexes **[$MoO_2(L_1D)$]- [$MoO_2(L_4D)$]**

Table 3

Selected bond length (A^0) for the ligands **H_2L_2** , **H_2L_3** and the complexes **[$MoO_2(L_1D)$] - [$MoO_2(L_4D)$]**

Table 4

Selected angles(^{0}) for the complexes **[$MoO_2(L_1D)$] - [$MoO_2(L_4D)$]**

Table 5

DNA binding constants [$K_b(M^{-1})$] of ligands and complexes

Table 6

IC_{50} (μM) of complexes **[$MoO_2(L_1D)$]- [$MoO_2(L_4D)$]**

Table 1

Crystallographic data for ligands $\mathbf{H_2L_2}$ and $\mathbf{H_2L_3}$

	$\mathbf{H_2L_2}$	$\mathbf{H_2L_3}$
Chemical formula	$C_{11}H_{15}N_3OS$	$C_{14}H_{21}N_3OS$
Formula weight	237.33	279.41
Crystal system	monoclinic	monoclinic
Crystal description	needle colorless	block colorless
Space group	$P2_1/c$	$P2_1/c$
Unit cell dimensions		
a (A^0)	12.2648(15)	21.2365(5)
b (A^0)	5.8340(5)	11.8745(3)
c (A^0)	16.8334(17)	12.2857(3)
α (^{0})	90	90
β (^{0})	99.177(9)	103.430(1)
γ (^{0})	90	90
Volume ($^0A^3$)	1189.1(2)	3013.40(13)
Z	4	8
D_{calc} (g/cm^3)	1.326	1.232
Crystal size (mm)	0.09 x 0.12 x 0.66	0.21 x 0.33 x 0.42
Temperature (K)	100	100
Total data	5007	34574
Unique data	2041	8833
R_{int}	0.082	0.049
Observed data [I>2σ(I)]	1390	5695
R_1	0.0912	0.0578
wR_2	0.2650	0.1503
S	1.11	1.04

Table 2

Crystallographic data for complexes **[$MoO_2(L_1D)$]- [$MoO_2(L_4D)$]**

	[$MoO_2(L_1D)$]	**[$MoO_2(L_2D)$]**	**[$MoO_2(L_3D)$]**	**[$MoO_2(L_4D)$]**
Chemical formula	$C_{10}H_{11}ClMoN_3O_4S$	$C_{12}H_{17}MoN_3O_4S$	$C_{15}H_{23}MoN_3O_4S$	$C_{11}H_{15}MoN_3O_5S$
Formula weight	400.68	395.30	437.37	397.27
Crystal system	monoclinic	monoclinic	triclinic	triclinic
Crystal description	block orange	needle brown	block orange	block brown
Space group	$P2_1/c$	$P2_1/c$	P - 1	P - 1
Unit cell dimensions				
a (A^0)	9.1511(2)	7.5722(5)	7.2726(1)	8.4428(1)
b (A^0)	9.5994(2)	18.9858(13)	9.5125(2)	9.1418(1)
c (A^0)	15.4786(3)	10.7452(7)	13.2894(3)	10.9457(1)
α (^{0})	90	90	89.244(1)	65.7400
β (^{0})	98.744(1)	108.701(1)	81.380(1)	70.665(1)
γ (^{0})	90	90	89.781(1)	81.547(1)
Volume ($^0A^3$)	1343.92(5)	1463.22(17)	908.90(3)	726.710(14)
Z	4	4	2	2
D_{calc} (g/cm^3)	1.980	1.794	1.598	1.816
Crystal size (mm)	0.18 x 0.32 x 0.45	0.05 x 0.10 x 0.58	0.10 x 0.14 x 0.39	0.14 x 0.22 x 0.28
Temperature (K)	100	100	100	100
Total data	18311	15913	23201	19631
Unique data	4897	4282	6510	5304
R_{int}	0.022	0.028	0.021	0.016
Observed data [I>2σ(I)]	4510	3877	6118	5138
R_1	0.0252	0.0218	0.0241	0.0163
wR_2	0.0752	0.0574	0.0579	0.0427
S	1.08	1.05	1.07	1.08

Table 3

Selected bond length (A^0) for the ligands **H_2L_2** , **H_2L_3** and the complexes **[$MoO_2(L_1D)$]** - **[$MoO_2(L_4D)$]**

	H_2L_2	H_2L_3		[$MoO_2(L_1D)$]	[$MoO_2(L_2D)$]	[$MoO_2(L_3D)$]	[$MoO_2(L_4D)$]
S1-C8	1.702(7)	1.6840(18)	**S1-C8**	1.7557(15)	1.7545(15)	1.7528(14)	1.7525(11)
N2-C8	1.337(8)	1.358(3)	**N2-C8**	1.3217(19)	1.3156(19)	1.3192(18)	1.3180(15)
N3-C8	1.350(8)	1.333(2)	**Mo-S1**	2.4346(4)	2.4285(5)	2.4356(4)	2.4253(3)
N1-C7	1.309(8)	1.294(2)	**Mo-O1**	1.9391(11)	1.9361(11) [a]	1.9268(11)	1.9288(9)
C1-O1	1.384(8)	1.365(2)	**Mo-O2**	2.3364(11) [b]	2.3559(12) [a]	2.3250(12)	2.3207(9)
N1-N2	1.399(7)	1.378(2)	**Mo-O3**	1.7076(12)	1.7136(12)	1.7081(11)	1.7157(8)
			Mo-O4	1.7043(12)	1.6975(13)	1.7022(12)	1.7042(9)
			Mo-N1	2.2961(12)	2.2795(13)	2.2795(12)	2.2782(9)

[a] O1=O4 , O2=O1

[b] O2=O4

Table 4

Selected angles(^{0}) for the complexes **[$MoO_2(L_1D)$]** - **[$MoO_2(L_4D)$]**.

	[$MoO_2(L_1D)$]	**[$MoO_2(L_2D)$]**	**[$MoO_2(L_3D)$]**	**[$MoO_2(L_4D)$]**
S1-Mo-O1	153.37(3)	153.14(4)	152.85(4) [a]	154.87(3)
S1-Mo-O2	82.36(3)	82.41(3) [b]	81.60(3) [a]	83.01(2)
S1-Mo-O3	91.50(4)	88.87(4)	90.51(4)	88.92(3)
S1-Mo-O4	95.21(4)	97.44(4)	96.21(4) [a]	96.04(3)
S1-Mo-N1	75.65(3)	75.74(3)	75.43(3)	76.13(3)
O1-Mo-O2	78.43(4)	76.97(5)	78.50(5)	78.77(4)
O1-Mo-O3	104.35(5)	106.12(5)	105.54(5)	106.20(4)
O1-Mo-O4	100.79(5)	99.67(6)	100.21(5)	99.01(4)
O1-Mo-N1	82.71(5)	83.40(5)	82.55(4)	83.30(3)
O2-Mo-O3	83.50(5)	85.09(5)	84.19(5)	84.35(4)
O2-Mo-O4	170.70(5)	169.31(5)	170.05(5)	170.28(4)
O2-Mo-N1	79.14(4)	78.60(4)	78.23(4)	78.29(3)
O3-Mo-O4	105.58(6)	105.60(6)	105.58(6)	105.32(4)
O3-Mo-N1	159.57(5)	158.81(5)	158.83(5)	158.25(4)
O4-Mo-N1	91.56(5)	90.99(5)	91.82(5)	92.08(4)

[a] O1=O4 , O2=O1 , O4=O2

[b] O2=O4

Table 5

DNA binding constants [K_b (M^{-1})] of ligands and complexes

Ligand	K_b	Complex	K_b
H_2L_1	5.051×10^4	**$[MoO_2(L_1D)]$**	1.407×10^6
H_2L_2	8.075×10^4	**$[MoO_2(L_2D)]$**	1.360×10^6
H_2L_3	3.174×10^5	**$[MoO_2(L_3D)]$**	1.559×10^6
H_2L_4	1.342×10^4	**$[MoO_2(L_4D)]$**	1.00×10^5

Table 6

IC_{50} (µM) of complexes **$[MoO_2(L_1D)]$**- **$[MoO_2(L_4D)]$**

Complex	IC_{50}
$[MoO_2(L_1D)]$	4.5
$[MoO_2(L_2D)]$	4.6
$[MoO_2(L_3D)]$	3.2
$[MoO_2(L_4D)]$	6.4
5-FU	7.3

Synthesis, crystal structure, Deoxyribose Nucleic Acid interaction and antitumor activity of some thiosemicarbazonatomolybdenum(VI)

Mouayed A. Hussein [a], Teoh S. Guan [a *], Rosenani A. Haque [a], Mohamed B. Khadeer Ahamed[b], Amin M.S. Abdul Majid[b]

[a] School of Chemical Science, Universiti Sains Malaysia, 11800 – Mindern, Pulau Pinang, Malaysia

[b] EMAN Research and Testing Laboratory, School of Pharmaceutical Sciences, Universiti Sains Malaysia, 11800 – Mindern, Pulau Pinang, Malaysia

*Corresponding author: Dr. Teoh Siang Guan, PhD,
Professor
School of Chemical Sciences
Universiti Sains Malaysia
Penang-11800, Malaysia
E-mail: sgteoh@usm.my
H/P : (604) – 6577888
Fax : (604) - 6574854

Graphical abstract

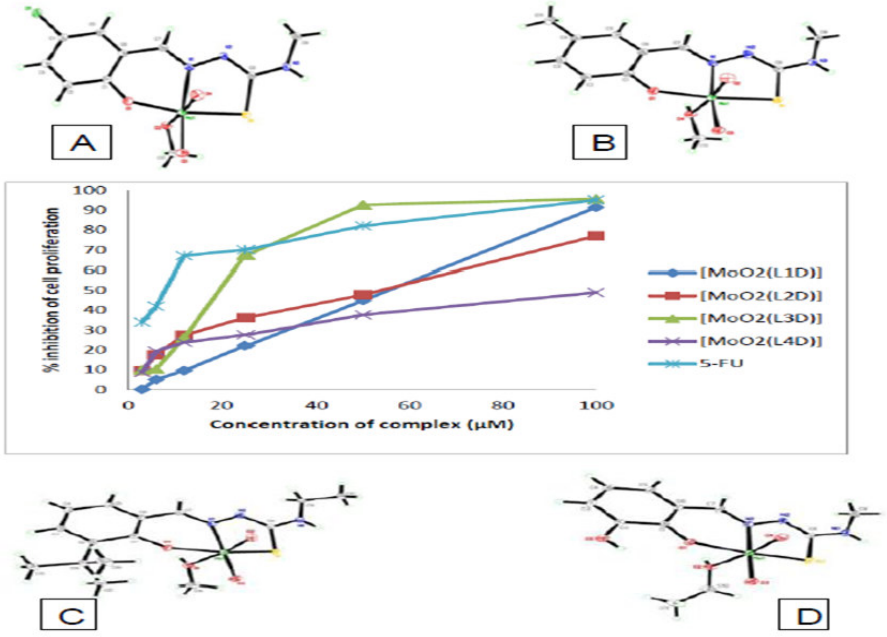

Percentage of cell proliferation inhibition by A= $[MoO_2(L_1D)]$, B= $[MoO_2(L_2D)]$, C= $[MoO_2(L_3D)]$ and D=$[MoO_2(L_4D)]$.

Antitumour activity of some thiosemicarbazonatomolybdenum(VI) complexes

► Four Schiff bases derived from 4-ethyl (methyl)thiosemicarbazone are synthesized

► All these ligands are coordinated with molybdenum(VI)

► The molecular structure of the complexes was determined by X-ray single crystal

► The complexes antitumour activity against HCT 116 cell line were investigated.